L. Dozio, L. Alimonti
Variable Kinematic Finite Element Models of Multilayered Composite Plates Coupled with Acoustic Fluid
Mechanics of Advanced Materials and Structures, Vol. 23, N. 9, 2016, p. 981-996
doi:10.1080/15376494.2015.1121558

Variable kinematic finite element models of multilayered composite plates coupled with acoustic fluid

Lorenzo Dozio Luca Alimonti*

Department of Aerospace Science and Technology
Politecnico di Milano, Milan, Italy

Abstract

This paper presents a novel and advanced finite element formulation of the structural-acoustic problem involving thin and thick multilayered composite plates coupled with a cavity. Exploiting the Carrera's unified formulation, many plate and fluid-structure interface elements based on different kinematic models including higher-order equivalent single-layer and layerwise theories are developed within a single mathematical framework. Accordingly, a large number of vibro-acoustic models can be easily obtained and selected according to the accuracy requirements of the application. In particular, it is shown that refined models can be adopted in those cases where models relying on traditional or low-order plate theories fail in providing the correct estimation of the fluid-structure coupling. The proposed formulation is also validated with respect to some reference cases available in the literature.

*currently at GAUS, Department of Mechanical Engineering, University of Sherbrooke, CA.

1 Introduction

It is well known that, whenever a flexible structure is in contact with a fluid, a so-called fluid-structure coupling interaction arises, such that the structure is subjected to a force loading due to the fluid pressure along the fluid-structure interface, and, at the same time, the pressure field in the fluid is affected by the motion of the elastic structural boundary [1]. In this work, the case when the structure undergoes linear vibrations and the fluid can be assumed to be compressible and inviscid is considered. The corresponding problem is known as structural-acoustic problem or coupled vibro-acoustic problem [2]. In particular, the system under study in this paper involves an enclosure completely filled with air and surrounded by a structure which can be elastic or perfectly rigid.

Over the last three decades, research on numerical modeling and analysis of structural-acoustic systems has been very active, especially in the automotive and aeronautical engineering fields [3, 4]. Indeed, increasing customer demand for improved comfort environments have prompted researchers into studying the fundamental phenomena governing the structural-acoustic coupling [5], with the aim of designing quieter vehicles and investigating novel techniques to reduce cabin interior noise levels [6, 7, 8].

Many numerical methods can be adopted to model structural-acoustic problems [9]. The approach used in this work is the finite-element (FE) method [10], which is also the most common technique in engineering practice, especially in the low-frequency range, where structural and acoustic wavelengths are long and the response spectra exhibit strong and regular modal behavior. Since both the structural and acoustic domains are modeled through finite elements, the corresponding formulation is denoted as FE/FE vibro-acoustic model [11].

The structural FE formulation is naturally based on the displacement field as the independent variable. On the contrary, there are multiple choices of the independent variable for the description of the fluid response, e.g., fluid displacement, pressure, velocity potential, displacement potential and combination of thereof [12, 13]. The most common approach, which is also adopted here, is to develop acoustic elements based on the scalar fluid pressure. The combination of displacement-based structural elements and pressure-based acoustic elements is known as (u, p) formulation of the structural-acoustic problem. This formulation has the drawback

of yielding non-symmetric matrices of the coupled system. In order to avoid non-symmetric solvers and reduce at the same time the model size, a modal coupling solution as described below is implemented [14, 15, 16].

Among interior structural-acoustic problems, one case of great interest involves an acoustic cavity with one or more faces consisting of flexible plates. A huge amount of work has been done in the past on the modeling and analysis of plate-cavity systems [17, 5, 18, 19, 20, 21]. The most important physical aspects and effects due to their coupling have been extensively presented and discussed. However, almost all the numerical studies available in the literature are limited to thin isotropic plates, which are discretized using finite elements based on traditional two-dimensional (2-D) plate theories, like classical plate theory (CPT) and first-order shear deformation theory (FSDT). Even when multilayered composite plates were considered, FE formulations of the elastic structure have been still restricted to FSDT models [22], which are viewed as equivalent single-layer (ESL) models of the laminate with appropriate average stiffness and mass properties. This choice is probably due to the need of working with relatively simple and economical structural models or to the availability of commercial finite element softwares where only FSDT-based elements are generally implemented.

The application of composite materials in the aerospace and automotive field has grown rapidly in the last decades. As a consequence, the coupling of composite structures with acoustic fluid represents an expanding research area. Indeed, multilayered composite plates can offer many advantages with respect to classical metallic constructions. It is also noted that interior cabin panels of modern vehicles are made of multiple layers of different materials for sound-proofing requirements. However, some complicating effects arise in the accurate modeling of multilayered plates, which are related to the large difference in the mechanical properties of the layers in the thickness direction [23, 24, 25, 26]. In particular, mechanical variables exhibit a so-called *zig-zag* distribution through the thickness, with strong variation of the local slope at each layer interface. Furthermore, anisotropic multilayered constructions are typically characterized by higher shear and normal deformability than isotropic one-layer structures. Such effects are amplified when the thickness ratio gets larger, the degree of orthotropy is high and shorter wavelengths are considered. CPT and FSDT are based on simplifying a priori assump-

tions which make them rather ineffective in accurately capturing the above effects. As a result, the corresponding finite element models can show great difficulties in providing the correct estimation of the dynamic behavior of the multilayered composite plate and, as a consequence, the accurate prediction of the coupled vibro-acoustic response.

Instead of resorting to a full three-dimensional (3-D) model of the structural field, which typically involves an unacceptable computational burden, the FE/FE vibro-acoustic model, if needed, can rely on plate and structural-acoustic interface elements based on refinements of classical 2-D plate theories. Broadly speaking, two main categories of refined plate theories can be envisaged [27, 28]. The first approach relies on enriching the FSDT model with higher-order terms as series expansion of the thickness coordinate. The highest power of the expansion is called order of the theory. In the second approach, a local independent first- or higher-order 2-D displacement field is postulated in each layer, and appropriate continuity conditions are enforced at layer interfaces. The first category encompasses so-called higher-order ESL theories, whereas models falling in the second category are denoted as layerwise (LW) or discrete-layer theories.

The main goal of this work is to present an advanced FE (u, p) formulation of the structural-acoustic problem involving both thin and thick multilayered composite plates modeled according to the refined theories mentioned so far. In this way, the resulting refined models can provide a more accurate approximation of the vibro-acoustic coupling than classical models based on CPT or FSDT. The proposed technique can be considered as an extension of the Carrera's unified formulation (CUF) to coupled plate-cavity systems. As originally presented in [29] and developed in many other papers (see, e.g., [30, 31, 32, 33, 34]), CUF is a powerful technique capable of handling, within the same mathematical framework, ESL and LW theories of variable order. Accordingly, a large number of refined models can be implemented without the need of writing from scratch a new mathematical formulation and a new numerical code each time an improved kinematic model is required. As a result, refined plate and fluid-structure interface elements based on different kinematic theories, called in the following *variable kinematic elements*, are developed. Through an extensive use of indicial notations, small invariant nodal-, layer- and order-independent mass, stiffness and structural-acoustic coupling matrices

are first derived. Such matrices, called *fundamental nuclei* of the present (u, p) formulation, represent the building blocks to obtain the finite element matrices of the coupled vibro-acoustic problem as shown in the following.

The paper is organized as follows. Section 2 gives an overview of the general equations describing the structural-acoustic problem under study and the corresponding variational formulation. Following the CUF approach, the variational formulation is discretized in Section 3 with variable kinematic finite elements and the final form of governing equations is presented. The resulting system is then solved in Section 4 through a modal coupling technique. The properties and capabilities of the proposed modeling tool are presented and discussed in Section 5 using some illustrative examples. Some conclusions are finally drawn in Section 6.

2 Structural-acoustic coupled problem

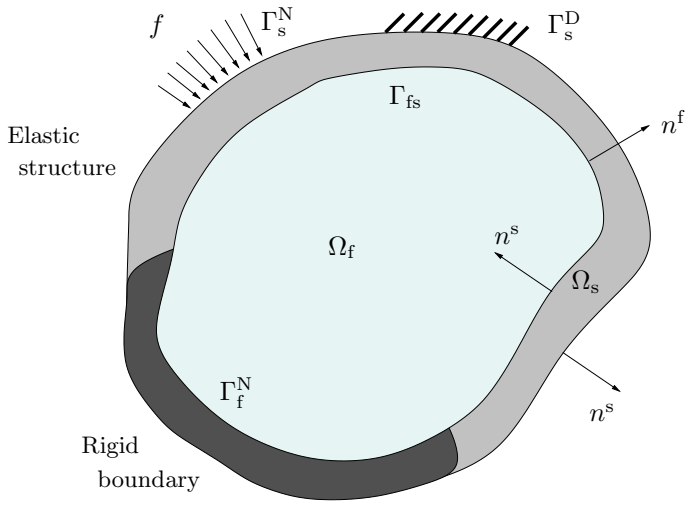

Figure 1: The structural-acoustic coupled problem under study.

The internal structural-acoustic coupled problem under study is represented in Figure 1. An elastic structure occupying the domain $\Omega_{\rm s}$ is in contact with a compressible inviscid acoustic fluid occupying the domain $\Omega_{\rm f}$. The fluid-structure interface is denoted by $\Gamma_{\rm fs}$ and $n_i^{\rm s}$ and $n_i^{\rm f}$ are the unit normals external to $\Omega_{\rm s}$ and $\Omega_{\rm f}$, respectively. The fluid can also have a rigid boundary where the condition of zero normal pressure gradient is imposed. The structure is subjected to a prescribed surface force density f_i on a part $\Gamma_{\rm s}^{\rm N}$ of its external boundary and to null displacements on the complementary part $\Gamma_{\rm s}^{\rm D}$.

2.1 Local equations

The 3-D local equations describing the dynamic behavior of the elastic structure are given by

$$\sigma_{ij,j} = \rho_{\mathrm{s}} \frac{\partial^2 u_i}{\partial t^2} \qquad \text{in} \quad \Omega_{\mathrm{s}} \tag{1a}$$

$$\sigma_{ij} n_j^{\mathrm{s}} = f_i \qquad \text{on} \quad \Gamma_{\mathrm{s}}^{\mathrm{N}} \tag{1b}$$

$$u_i = 0 \qquad \text{on} \quad \Gamma_{\mathrm{s}}^{\mathrm{D}} \tag{1c}$$

$$\sigma_{ij} n_j^{\mathrm{s}} = p\, n_i^{\mathrm{f}} \qquad \text{on} \quad \Gamma_{\mathrm{fs}} \tag{1d}$$

where ρ_{s} is the mass density and a comma subscript denotes partial derivative. Note that the usual summation convention for repeated indices has been adopted. Eq. (1a) is the classical equation of elastodynamics in terms of the stress tensor σ_{ij} and the displacement field components u_i, Eqs. (1b) and (1c) represent the prescribed Neumann and Dirichlet mechanical boundary conditions on $\Gamma_{\mathrm{s}}^{\mathrm{N}}$ and Γ_s^{D}, respectively, and Eq. (1d) arises from the pressure p of the fluid acting on the elastic structure in correspondence with the fluid-structure interface. The elastic structure is supposed to have a linear elastic behavior. Accordingly, the stress tensor is related to the small strain tensor ε_{ij} by the constitutive law

$$\sigma_{ij} = C_{ijkl} \varepsilon_{kl} \tag{2}$$

where C_{ijkl} denotes the material stiffness coefficient. The strain components are in turn related to the displacement components by the following gradient relations

$$\varepsilon_{ij} = \frac{1}{2} \left(u_{i,j} + u_{j,i} \right) \tag{3}$$

Since the internal fluid is assumed to be inviscid, its motion can be described by using the pressure scalar field p. In absence of acoustic sources, the response of the fluid to a prescribed arbitrary normal motion of the fluid-structure interface is governed by the following set of

equations

$$p_{,ii} = \frac{1}{c_\mathrm{f}^2}\frac{\partial^2 p}{\partial t^2} \qquad \text{in} \quad \Omega_\mathrm{f} \tag{4a}$$

$$p_{,i} n_i^\mathrm{f} = -\rho_\mathrm{f}\frac{\partial^2 u_i}{\partial t^2} n_i^\mathrm{f} \qquad \text{on} \quad \Gamma_\mathrm{fs} \tag{4b}$$

$$p_{,i} n_i^\mathrm{f} = 0 \qquad \text{on} \quad \Gamma_\mathrm{f}^\mathrm{N} \tag{4c}$$

where ρ_f is the mass density of the fluid and c_f is the constant speed of sound in the fluid. The last equation (4c) expresses the zero normal pressure gradient on the rigid walled boundary $\Gamma_\mathrm{f}^\mathrm{N}$.

2.2 Variational formulation

The (u, p) variational formulation associated with the previous local equations can be obtained by the test-function method.

Considering first the elastodynamic problem, Eq. (1a) is multiplied by an arbitrary test-function δu_i belonging to the space of sufficiently regular functions u_i defined in Ω_s such that $u_i = 0$ on $\Gamma_\mathrm{s}^\mathrm{D}$. After integrating over the structural domain and applying the Green's formula, we obtain

$$\int_{\Omega_\mathrm{s}} \delta\varepsilon_{ij}\sigma_{ij}\,\mathrm{d}v + \int_{\Omega_\mathrm{s}} \delta u_i \rho_\mathrm{s}\frac{\partial^2 u_i}{\partial t^2}\,\mathrm{d}v = \int_{\Gamma_\mathrm{s}^\mathrm{N}} \delta u_i f_i\,\mathrm{d}s + \int_{\Gamma_\mathrm{fs}} \delta u_i p n_i^\mathrm{f}\,\mathrm{d}s \tag{5}$$

where the right-hand side takes into account the boundary conditions in Eq. (1b) and (1d).

The same procedure is applied to the acoustic problem in Eqs. (4a-4c). Multiplying the acoustic wave equation by an arbitrary test-function δp belonging to the space of sufficiently regular functions p defined in Ω_f, applying Green's formula and taking into account Eq. (4b) yields

$$\int_{\Omega_\mathrm{f}} \delta p_{,i} p_{,i}\,\mathrm{d}v + \frac{1}{c_\mathrm{f}^2}\int_{\Omega_\mathrm{f}} \delta p\,\frac{\partial^2 p}{\partial t^2}\,\mathrm{d}v = -\int_{\Gamma_\mathrm{fs}} \delta p\,\rho_\mathrm{f}\frac{\partial^2 u_i}{\partial t^2} n_i^\mathrm{f}\,\mathrm{d}s \tag{6}$$

3 Finite element discretization

The above variational formulation can be discretized by the finite element method. In this section, the discretization procedure is specifically applied to an elastic structure consisting of a plate made of N_ℓ layers of orthotropic material. Without any loss of generality, the plate is assumed to be in contact with the acoustic fluid at its bottom surface and the layers are numbered starting from the bottom layer of the laminate. The following mathematical formulation encompasses both thin to thick multilayered plates which are modeled according to advanced 2-D kinematic theories, as explained below.

3.1 Vector form of the variational formulation

First, the 3-D displacement vector $\mathbf{u}^k = \left\{u^k \; v^k \; w^k\right\}^{\mathrm{T}}$ of the k-th layer is introduced, where u and v denote in-plane displacements along x and y direction of the plate, respectively, and w is the displacement in the thickness direction z. Assuming an arbitrary load vector $\mathbf{f}$ acting on the plane Γ_{s}^k at coordinate $\bar{z}$ of layer ℓ of the plate ($\ell = 1, \ldots, N_\ell$), Eq. (5) can be written in vector form as follows

$$\begin{aligned}\sum_{k=1}^{N_\ell} \int_{\Omega_{\mathrm{s}}^k} \left(\delta\boldsymbol{\varepsilon}_{\mathrm{p}}^{k^{\mathrm{T}}} \boldsymbol{\sigma}_{\mathrm{p}}^k + \delta\boldsymbol{\varepsilon}_{\mathrm{n}}^{k^{\mathrm{T}}} \boldsymbol{\sigma}_{\mathrm{n}}^k\right) \mathrm{d}v + \sum_{k=1}^{N_\ell} \int_{\Omega_{\mathrm{s}}^k} \delta\mathbf{u}^{k^{\mathrm{T}}} \rho_{\mathrm{s}} \frac{\partial^2 \mathbf{u}^k}{\partial t^2} \mathrm{d}v = \\ \sum_{k=1}^{N_\ell} \delta_{k\ell} \int_{\Gamma_{\mathrm{s}}^k} \delta\mathbf{u}^{k^{\mathrm{T}}}(\bar{z})\, \mathbf{f}\, \mathrm{d}s + \sum_{k=1}^{N_\ell} \delta_{k1} \int_{\Gamma_{\mathrm{fs}}} \delta\mathbf{u}^{k^{\mathrm{T}}}(z_{\mathrm{fs}})\, p\, \mathbf{n}\, \mathrm{d}s\end{aligned} \tag{7}$$

where Ω_{s}^k is the domain of k-th layer, z_{fs} is the coordinate of the fluid-structure interface, i.e., the bottom of the plate, $\delta_{k\ell}$ is the Kronecker delta which is non null only if $k = \ell$, and δ_{k1} is the Kronecker delta which is non null only for the bottom layer of the plate ($k = 1$). The stress and strain vectors have been split into in-plane and out-of-plane (normal) components as follows

$$\boldsymbol{\sigma}_{\mathrm{p}}^k = \left\{\begin{array}{c}\sigma_{xx}^k \\ \sigma_{yy}^k \\ \sigma_{xy}^k\end{array}\right\}, \qquad \boldsymbol{\sigma}_{\mathrm{n}}^k = \left\{\begin{array}{c}\sigma_{xz}^k \\ \sigma_{yz}^k \\ \sigma_{zz}^k\end{array}\right\}, \qquad \boldsymbol{\epsilon}_{\mathrm{p}}^k = \left\{\begin{array}{c}\epsilon_{xx}^k \\ \epsilon_{yy}^k \\ \gamma_{xy}^k\end{array}\right\}, \qquad \boldsymbol{\epsilon}_{\mathrm{n}}^k = \left\{\begin{array}{c}\gamma_{xz}^k \\ \gamma_{yz}^k \\ \epsilon_{zz}^k\end{array}\right\} \tag{8}$$

Therefore, the constitutive law of the k-th layer is written as

$$\begin{aligned} \boldsymbol{\sigma}_{\mathrm{p}}^{k} &= \mathbf{C}_{\mathrm{pp}}^{k}\boldsymbol{\varepsilon}_{\mathrm{p}}^{k} + \mathbf{C}_{\mathrm{pn}}^{k}\boldsymbol{\varepsilon}_{\mathrm{n}}^{k} \\ \boldsymbol{\sigma}_{\mathrm{n}}^{k} &= \mathbf{C}_{\mathrm{np}}^{k}\boldsymbol{\varepsilon}_{\mathrm{p}}^{k} + \mathbf{C}_{\mathrm{nn}}^{k}\boldsymbol{\varepsilon}_{\mathrm{n}}^{k} \end{aligned} \tag{9}$$

where the matrices of stiffness coefficients are expressed in the plate reference system through a proper coordinate transformation, if needed, from the corresponding coefficients in the layer reference system [35].

Similarly, the vector form of the fluid problem in Eq. (6) is written as follows

$$\int_{\Omega_{\mathrm{f}}} \delta\nabla p^{\mathrm{T}}\nabla p \,\mathrm{d}v + \frac{1}{c_{\mathrm{f}}^{2}}\int_{\Omega_{\mathrm{f}}} \delta p \,\frac{\partial^{2} p}{\partial t^{2}}\,\mathrm{d}v + \sum_{k=1}^{N_{\ell}} \delta_{k1}\int_{\Gamma_{\mathrm{fs}}} \delta p \,\rho_{\mathrm{f}}\,\mathbf{n}^{\mathrm{T}}\frac{\partial^{2}\mathbf{u}^{k}}{\partial t^{2}}(z_{\mathrm{fs}})\,\mathrm{d}s = 0 \tag{10}$$

3.2 Variable kinematic models of the multilayered plate

According to the formulation proposed by Carrera [29], an entire class of 2-D refined LW plate theories (see Figure 2(a)) can be employed by expressing the mechanical displacement vector $\mathbf{u}^{k}$ through the following notation

$$\mathbf{u}^{k}(x, y, \zeta_{k}, t) = F_{\alpha}(\zeta_{k})\mathbf{u}_{\alpha}^{k}(x, y, t) \tag{11}$$

where α is the so-called theory-related index, $F_{\alpha}(\zeta_{k})$ are thickness functions defined with respect to the local layer coordinate ζ_{k}, and $\mathbf{u}_{\alpha}^{k}(x, y, t) = \left\{u_{\alpha}^{k}(x, y, t)\ v_{\alpha}^{k}(x, y, t)\ w_{\alpha}^{k}(x, y, t)\right\}^{\mathrm{T}}$ is the vector of 2-D generalized kinematic coordinates involved in the assumed displacement model corresponding to index α. An infinite number of theories of different order can be implemented by selecting in Eq. (11) the set of thickness functions and the range values of α. A family of layer-wise theories of variable order N is here considered by assuming $\alpha = t, b, r$ $(r = 2, \ldots, N)$ and selecting

$$F_{t}(\zeta_{k}) = \frac{1+\zeta_{k}}{2}; \qquad F_{b}(\zeta_{k}) = \frac{1-\zeta_{k}}{2}; \qquad F_{r}(\zeta_{k}) = P_{r}(\zeta_{k}) - P_{r-2}(\zeta_{k}) \tag{12}$$

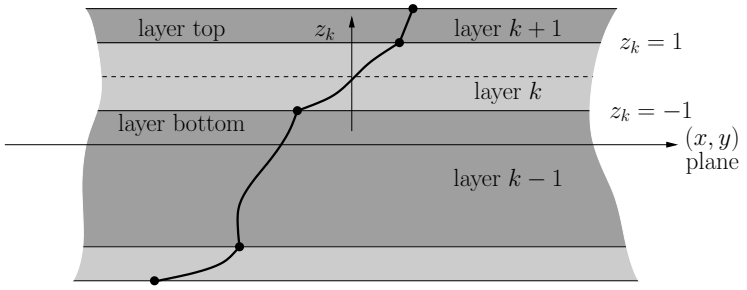

(a) Layerwise model

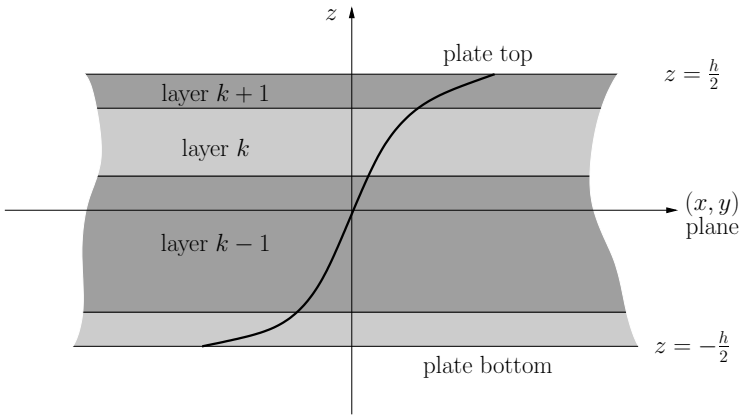

(b) Equivalent single-layer model

Figure 2: Example of through-the-thickness distribution of displacements in case of higher-order layerwise and equivalent single-layer plate theories.

where $P_r(\zeta_k)$ is the Legendre polynomial of r-th order. Accordingly, the displacement variables $\mathbf{u}_b^k$ and $\mathbf{u}_t^k$ are the values at the bottom and top surfaces of k-th layer, respectively, and the inter-laminar displacement continuity can be easily imposed as $\mathbf{u}_t^k = \mathbf{u}_b^{k+1}$ for $k = 1, 2, \ldots, N_\ell - 1$. Following the CUF nomenclature, each member of the family is shortly denoted here by the acronym LDN, which stands for (L)ayer-wise (D)isplacement-based theory of order N. The number of kinematic degrees of freedom associated with the theory LDN is given by $3(N+1)N_\ell - 3(N_\ell - 1)$.

The formal approach adopted in Eq. (11) can be also used to define a class of ESL plate theories (see Figure 2(b)). Since in this case the kinematics is layer-independent, the k index in Eq. (11) is dropped and a set of global thickness functions F_α is selected. The classical z expansion is here adopted in terms of Taylor polynomials by assuming

$$F_\alpha = z^\alpha \tag{13}$$

where now $t = 0$ and $b = 1$. The related N-order ESL theory is denoted by the acronym EDN, which stands for (E)quivalent single-layer (D)isplacement-based theory of order N. As such, the number of degrees of freedom for a EDN theory is $3(N + 1)$.

Inserting the assumed displacement field of Eq. (11) into the gradient relations in Eq. (3), the in-plane and normal strains can be expressed as follows

$$\begin{aligned} \boldsymbol{\varepsilon}_{\mathrm{p}}^{k} &= F_{\alpha} \boldsymbol{\mathcal{D}}_{\mathrm{p}} \mathbf{u}_{\alpha}^{k} \\ \boldsymbol{\varepsilon}_{\mathrm{n}}^{k} &= F_{\alpha} \boldsymbol{\mathcal{D}}_{\mathrm{n}} \mathbf{u}_{\alpha}^{k} + \frac{\partial}{\partial z} F_{\alpha} \mathbf{u}_{\alpha}^{k} \end{aligned} \tag{14}$$

where

$$\boldsymbol{\mathcal{D}}_{\mathrm{p}} = \begin{bmatrix} \partial/\partial x & 0 & 0 \\ 0 & \partial/\partial y & 0 \\ \partial/\partial y & \partial/\partial x & 0 \end{bmatrix}, \qquad \boldsymbol{\mathcal{D}}_{\mathrm{n}} = \begin{bmatrix} 0 & 0 & \partial/\partial x \\ 0 & 0 & \partial/\partial y \\ 0 & 0 & 0 \end{bmatrix}$$

3.3 Nodal coordinates and shape functions

According to the previous plate modeling, a 2-D finite element discretization of the elastic domain is employed by expressing the mechanical kinematic coordinates $\mathbf{u}_{\alpha}^{k}$ related to the selected theory in terms of generalized nodal coordinates $\mathbf{d}_{\alpha i}^{k}$ as follows

$$\mathbf{u}_{\alpha}^{k}(x, y, t) = N_{i}^{\mathrm{s}}(x, y) \mathbf{d}_{\alpha i}^{k}(t) \qquad (i = 1, \ldots, N_{n}^{\mathrm{s}}) \tag{15}$$

where N_{n}^{s} is the number of nodes in the 2-D structural element and N_{i}^{s} are appropriate shape functions for the structural part. Note that the summation convention is also introduced in Eq. (15) on the index i. Four-node ($N_{n}^{\mathrm{s}} = 4$) quadrilateral plate elements [10] are implemented in this work with the following linear interpolating functions

$$\begin{Bmatrix} N_{1}^{\mathrm{s}} \\ N_{2}^{\mathrm{s}} \\ N_{3}^{\mathrm{s}} \\ N_{4}^{\mathrm{s}} \end{Bmatrix} = \frac{1}{4} \begin{Bmatrix} (1-\xi)(1-\eta) \\ (1+\xi)(1-\eta) \\ (1+\xi)(1+\eta) \\ (1-\xi)(1+\eta) \end{Bmatrix}$$

expressed in terms of the element coordinates ξ and η varying from -1 to $+1$.

The fluid domain is discretized by 3-D acoustic elements [11]. The pressure p inside each element is expressed in terms of nodal pressures p_m as follows

$$p(x,y,z,t) = N_m^{\mathrm{a}}(x,y,z)p_m(t) \qquad\qquad (m = 1,\ldots,N_n^{\mathrm{a}}) \tag{16}$$

where N_n^{a} is the number of nodes and N_m^{a} are the shape functions for the acoustic part. Eight-nodes ($N_n^{\mathrm{a}} = 8$) hexahedral elements are implemented with the following linear shape functions

$$N_m^{\mathrm{a}} = \frac{1}{8}(1+\xi_m\xi)(1+\eta_m\eta)(1+\zeta_m\zeta)$$

in which ξ_m, η_m and ζ_m denote the local corner coordinates of the hexahedron.

3.4 Nodal equations at layer level

The indicial framework introduced thus far yields a set of finite element equations which can be expressed in terms of layer-level invariant matrices, called *fundamental nuclei* of the formulation [23], related to those quantities in the variational forms (7) and (10) which involve the mechanical displacements.

Let's first consider the structural problem. After inserting Eqs. (9) into Eq. (7), expressing the strains through Eq. (14) and using the finite element approximations in Eq. (15) and (16), the arbitrariness of the virtual variation of the mechanical nodal coordinates leads to the following set of nodal equations for each layer k of the plate

$$\delta\mathbf{d}_{\alpha i}^k : \qquad \mathbf{M}_{\alpha\beta ij}^k \frac{\mathrm{d}^2\mathbf{d}_{\beta j}^k}{\mathrm{d}t^2} + \mathbf{K}_{\alpha\beta ij}^k \mathbf{d}_{\beta j}^k - \mathbf{S}_{\alpha in}^k p_n = \mathbf{f}_{\alpha i}^k \tag{17}$$

where

$$\mathbf{M}_{\alpha\beta ij}^k = E_{\alpha\beta}^k \int_{\Gamma_{\mathrm{e}}^k} \rho_{\mathrm{s}}^k N_i^{\mathrm{s}} N_j^{\mathrm{s}} \mathbf{I}_3 \,\mathrm{d}A \tag{18}$$

is called nucleus of the structural mass,

$$\begin{aligned}\mathbf{K}^k_{\alpha\beta ij} = E^k_{\alpha\beta}\int_{\Gamma^k_{\mathrm{e}}}\Big[&(\boldsymbol{\mathcal{D}}_{\mathrm{p}}N^{\mathrm{s}}_i)^{\mathrm{T}}\,\mathbf{C}^k_{\mathrm{pp}}\left(\boldsymbol{\mathcal{D}}_{\mathrm{p}}N^{\mathrm{s}}_j\right)+(\boldsymbol{\mathcal{D}}_{\mathrm{p}}N^{\mathrm{s}}_i)^{\mathrm{T}}\,\mathbf{C}^k_{\mathrm{pn}}\left(\boldsymbol{\mathcal{D}}_{\mathrm{n}}N^{s}_j\right)\\ &+(\boldsymbol{\mathcal{D}}_{\mathrm{n}}N^{\mathrm{s}}_i)^{\mathrm{T}}\,\mathbf{C}^k_{\mathrm{np}}\left(\boldsymbol{\mathcal{D}}_{\mathrm{p}}N^{\mathrm{s}}_j\right)+(\boldsymbol{\mathcal{D}}_{\mathrm{n}}N^{\mathrm{s}}_i)^{\mathrm{T}}\,\mathbf{C}^k_{\mathrm{nn}}\left(\boldsymbol{\mathcal{D}}_{\mathrm{n}}N^{\mathrm{s}}_j\right)\Big]\mathrm{d}A\\ &+E^k_{\alpha_{,z}\beta}\int_{\Gamma^k_{\mathrm{e}}}\Big[N^{\mathrm{s}}_i\mathbf{C}^k_{\mathrm{np}}\left(\boldsymbol{\mathcal{D}}_{\mathrm{p}}N^{\mathrm{s}}_j\right)+N^{\mathrm{s}}_i\mathbf{C}^k_{\mathrm{nn}}\left(\boldsymbol{\mathcal{D}}_{\mathrm{n}}N^{\mathrm{s}}_j\right)\Big]\mathrm{d}A\\ &+E^k_{\alpha\beta_{,z}}\int_{\Gamma^k_{\mathrm{e}}}\Big[(\boldsymbol{\mathcal{D}}_{\mathrm{p}}N^{\mathrm{s}}_i)^{\mathrm{T}}\,\mathbf{C}^k_{\mathrm{pn}}N^{\mathrm{s}}_j+(\boldsymbol{\mathcal{D}}_{\mathrm{n}}N^{\mathrm{s}}_i)^{\mathrm{T}}\,\mathbf{C}^k_{\mathrm{nn}}N^{\mathrm{s}}_j\Big]\mathrm{d}A\\ &+E^k_{\alpha_{,z}\beta_{,z}}\int_{\Gamma^k_{\mathrm{e}}}N^{\mathrm{s}}_i\mathbf{C}^k_{\mathrm{nn}}N^{\mathrm{s}}_j\mathrm{d}A\end{aligned}\tag{19}$$

is called nucleus of the structural stiffness,

$$\mathbf{S}^k_{\alpha in}=\delta_{k1}F_\alpha(z_{\mathrm{fs}})\int_{\Gamma_{\mathrm{fs}}}N^{\mathrm{s}}_iN^{\mathrm{a}}_n(z_{\mathrm{fs}})\,\mathbf{n}\,\mathrm{d}A\tag{20}$$

is the nucleus of the structural-acoustic coupling, and

$$\mathbf{f}^k_{\alpha i}=\delta_{k\ell}F_\alpha(\bar{z})\int_{\Gamma^k_{\mathrm{e}}}N^{\mathrm{s}}_i\,\mathbf{f}\,\mathrm{d}A\tag{21}$$

is the nucleus related to the generalized mechanical load applied onto the plate. In the above definitions, $\mathbf{I}_3$ is the 3×3 identity matrix and the following thickness integrals have been introduced for each layer k

$$E^k_{\alpha\beta}=\int_{z_k}^{z_{k+1}}F_\alpha F_\beta\,\mathrm{d}z\qquad E^k_{\alpha_{,z}\beta}=\int_{z_k}^{z_{k+1}}F_{\alpha,z}F_\beta\,\mathrm{d}z$$

$$E^k_{\alpha\beta_{,z}}=\int_{z_k}^{z_{k+1}}F_\alpha F_{\beta,z}\,\mathrm{d}z\qquad E^k_{\alpha_{,z}\beta_{,z}}=\int_{z_k}^{z_{k+1}}F_{\alpha,z}F_{\beta,z}\,\mathrm{d}z$$

Note that the mass and stiffness nuclei $\mathbf{M}^k_{\alpha\beta ij}$ and $\mathbf{K}^k_{\alpha\beta ij}$ are 3×3 matrices written in compact form for each layer k, each pair (α,β) of theory-related indices, and each nodal pair (i,j). Therefore, they are invariant with respect to the number of layers of the laminated plate, the order N of the assumed plate theory and the number of nodes of the element. The same invariance property is also true for the 3×1 nucleus of the structural-acoustic coupling $\mathbf{S}^k_{\alpha in}$ and the 3×1 nucleus $\mathbf{f}^k_{\alpha i}$ related to the applied load.

It is also noted that the indicial form of Eq. (17) implies summation for repeated indices, which gives rise to the governing equations of the plate and fluid-structure interface element expressed through the related finite element matrices. However, the extended form of Eq. (17) is never explicitly written down since a direct expansion and assembly-like procedure of the nuclei is carried out. This procedure, as explained in the next section, fully exploits the invariance of the fundamental nuclei and allows building in an unified formulation different plate elements having variable kinematics capability.

Similarly to what done for the structural problem, the discretization of the acoustic problem can be expressed by the following nodal equations in indicial form

$$\delta p_m : \qquad \mathrm{Q}_{mn}\frac{\mathrm{d}^2 p_n}{\mathrm{d}t^2} + \mathrm{H}_{mn}p_n + \rho_\mathrm{f}\mathbf{R}^k_{m\beta j}\frac{\mathrm{d}^2\mathbf{d}^k_{\beta j}}{\mathrm{d}t^2} = 0 \tag{22}$$

where

$$\mathrm{Q}_{mn} = \frac{1}{c^2_\mathrm{a}}\int_{\Omega^e_f} N^\mathrm{a}_m N^\mathrm{a}_n \,\mathrm{d}V \tag{23}$$

can be considered as the scalar nucleus related to the acoustic mass,

$$\mathrm{H}_{mn} = \int_{\Omega^e_f} N^\mathrm{a}_{m,l} N^\mathrm{a}_{n,l} \,\mathrm{d}V \qquad (l = x, y, z) \tag{24}$$

is the scalar nucleus related to the acoustic stiffness, and

$$\mathbf{R}^k_{m\beta j} = \delta_{k1} F_\beta(z_\mathrm{fs}) \int_{\Gamma_\mathrm{fs}} \mathbf{n}^\mathrm{T} N^\mathrm{a}_m(z_\mathrm{fs}) N^\mathrm{s}_j \,\mathrm{d}A \tag{25}$$

is the 1×3 nucleus of the acoustic-structural coupling.

3.5 Assembly from nuclei to element matrices

As outlined in the previous section, the fundamental nuclei are the building blocks to obtain the finite element matrices of the structural-acoustic problem. The procedure involves the following steps:

1. The 3×3 nuclei $\mathbf{M}^k_{\alpha\beta ij}$ and $\mathbf{K}^k_{\alpha\beta ij}$ are expanded by varying the indices α, β over the

prescribed range according to the selected order N of the theory. The following $3(N+1)\times 3(N+1)$ layer-level nodal matrices are obtained

$$\mathbf{M}_{ij}^{k}=\begin{bmatrix}\mathbf{M}_{ttij}^{k} & \mathbf{M}_{trij}^{k} & \mathbf{M}_{tbij}^{k}\\ \mathbf{M}_{rtij}^{k} & \mathbf{M}_{rrij}^{k} & \mathbf{M}_{rbij}^{k}\\ \mathbf{M}_{btij}^{k} & \mathbf{M}_{brij}^{k} & \mathbf{M}_{bbij}^{k}\end{bmatrix}\qquad \mathbf{K}_{ij}^{k}=\begin{bmatrix}\mathbf{K}_{ttij}^{k} & \mathbf{K}_{trij}^{k} & \mathbf{K}_{tbij}^{k}\\ \mathbf{K}_{rtij}^{k} & \mathbf{K}_{rrij}^{k} & \mathbf{K}_{rbij}^{k}\\ \mathbf{K}_{btij}^{k} & \mathbf{K}_{brij}^{k} & \mathbf{K}_{bbij}^{k}\end{bmatrix} \tag{26}$$

where $r=2,\ldots,N$.

2. The 3×1 nuclei $\mathbf{S}_{\alpha in}^{k}$ and $\mathbf{f}_{\alpha i}^{k}$ and the 1×3 nucleus $\mathbf{R}_{m\beta j}^{k}$ are expanded accordingly by varying the index α and the index β, respectively, to obtain the following layer-level structural-acoustic coupling nodal matrices and load vector

$$\mathbf{S}_{in}^{k}=\begin{bmatrix}\mathbf{S}_{tin}^{k}\\ \mathbf{S}_{rin}^{k}\\ \mathbf{S}_{bin}^{k}\end{bmatrix}\qquad \mathbf{R}_{mj}^{k}=\begin{bmatrix}\mathbf{R}_{mtj}^{k} & \mathbf{R}_{mrj}^{k} & \mathbf{R}_{mbj}^{k}\end{bmatrix}\qquad \mathbf{f}_{i}^{k}=\begin{bmatrix}\mathbf{f}_{ti}^{k}\\ \mathbf{f}_{ri}^{k}\\ \mathbf{f}_{bi}^{k}\end{bmatrix} \tag{27}$$

3. Resulting matrices are assembled from layer to multilayer level according to the typology of the plate theory.

   (a) In the case of ESL theories, since the mechanical displacements are layer-independent, the layer-level matrices are simply accumulated layer by layer to give the following multilayer nodal matrices

   $$\mathbf{M}_{ij}=\sum_{k=1}^{N_\ell}\mathbf{M}_{ij}^{k}\qquad \mathbf{K}_{ij}=\sum_{k=1}^{N_\ell}\mathbf{K}_{ij}^{k}\qquad \mathbf{S}_{in}=\sum_{k=1}^{N_\ell}\mathbf{S}_{in}^{k}\qquad \mathbf{R}_{mj}=\sum_{k=1}^{N_\ell}\mathbf{R}_{mj}^{k} \tag{28}$$

   and multilayer nodal load vector

   $$\mathbf{f}_{i}=\sum_{k=1}^{N_\ell}\mathbf{f}_{i}^{k} \tag{29}$$

   (b) In the case of LW theories, according to the assumed discrete-layer kinematics, the matrices are assembled by enforcing the interlaminar continuity condition $\mathbf{u}_{t}^{k}=$

$\mathbf{u}_b^{k+1}$. For example, the multilayer nodal mass matrix is assembled as follows

$$\mathbf{M}_{ij} = \begin{bmatrix} \ddots & & & & & & \\ & \mathbf{M}_{rtij}^{k+1} & \mathbf{M}_{rrij}^{k+1} & \mathbf{M}_{rbij}^{k+1} & & & \\ & \mathbf{M}_{btij}^{k+1} & \mathbf{M}_{brij}^{k+1} & \mathbf{M}_{bbij}^{k+1} + \mathbf{M}_{ttij}^{k} & \mathbf{M}_{trij}^{k} & \mathbf{M}_{tbij}^{k} & \\ & & & \mathbf{M}_{rtij}^{k} & \mathbf{M}_{rrij}^{k} & \mathbf{M}_{rbij}^{k} & \\ & & & & & & \ddots \end{bmatrix} \tag{30}$$

The same is done for the multilayer stiffness matrix. The assembly-like procedure for the matrices expressing the structural-acoustic coupling yields

$$\mathbf{S}_{in} = \begin{bmatrix} \vdots \\ \mathbf{S}_{rin}^{k+1} \\ \mathbf{S}_{bin}^{k+1} + \mathbf{S}_{tin}^{k} \\ \mathbf{S}_{rin}^{k} \\ \vdots \end{bmatrix} \tag{31}$$

and

$$\mathbf{R}_{mj} = \begin{bmatrix} \dots & \mathbf{R}_{mbj}^{k+1} + \mathbf{R}_{mtj}^{k} & \mathbf{R}_{mrj}^{k} & \mathbf{R}_{mbj}^{k} + \mathbf{R}_{mtj}^{k-1} & \dots \end{bmatrix} \tag{32}$$

4. A final expansion is performed on the previous multilayer nodal matrices by varying the indices i, j from one to the number of nodes N_n^{s} of the structural element and the indices m, n from one to the number of nodes N_n^{f} of the fluid element. According to the quadrilateral and hexahedral elements used in this work, the following element matrices are obtained

$$\mathbf{M} = \begin{bmatrix} \mathbf{M}_{11} & \dots & \mathbf{M}_{14} \\ \vdots & & \vdots \\ \mathbf{M}_{41} & \dots & \mathbf{M}_{44} \end{bmatrix} \qquad \mathbf{K} = \begin{bmatrix} \mathbf{K}_{11} & \dots & \mathbf{K}_{14} \\ \vdots & & \vdots \\ \mathbf{K}_{41} & \dots & \mathbf{K}_{44} \end{bmatrix} \tag{33}$$

$$\mathbf{S} = \begin{bmatrix} \mathbf{S}_{11} & \dots & \mathbf{S}_{18} \\ \vdots & & \vdots \\ \mathbf{S}_{41} & \dots & \mathbf{M}_{48} \end{bmatrix} \qquad \mathbf{f} = \begin{bmatrix} \mathbf{f}_1 \\ \vdots \\ \mathbf{f}_4 \end{bmatrix} \qquad \mathbf{R} = \begin{bmatrix} \mathbf{R}_{11} & \dots & \mathbf{R}_{14} \\ \vdots & & \vdots \\ \mathbf{R}_{81} & \dots & \mathbf{R}_{84} \end{bmatrix} \tag{34}$$

It is noted that $\mathbf{R} = \mathbf{S}^{\mathrm{T}}$ and the structural mass and stiffness matrices are symmetric. An example involving the overall procedure to obtain the stiffness matrix of the quadrilateral plate element for a two-layered ($N_\ell = 2$) plate modeled using a second-order layerwise theory (LD2) is sketchily depicted in Figure 3.

5. By varying the indices m, n, the symmetric acoustic mass and stiffness matrices $\mathbf{Q}$ and $\mathbf{H}$ of the fluid element are also obtained.

3.6 Final form of governing equations

Once the element matrices are obtained as shown above, they can be assembled in the classical way according to 2-D structural and 3-D acoustic meshes. As a result, the global structural-acoustic coupled problem is described by the following set of equations

$$\begin{bmatrix} \mathbf{M} & \mathbf{0} \\ \rho_{\mathrm{f}}\mathbf{S}^{\mathrm{T}} & \mathbf{Q} \end{bmatrix} \begin{Bmatrix} \dfrac{\mathrm{d}^2\mathbf{d}}{\mathrm{d}t^2} \\ \dfrac{\mathrm{d}^2\mathbf{p}}{\mathrm{d}t^2} \end{Bmatrix} + \begin{bmatrix} \mathbf{K} & -\mathbf{S} \\ \mathbf{0} & \mathbf{H} \end{bmatrix} \begin{Bmatrix} \mathbf{d} \\ \mathbf{p} \end{Bmatrix} = \begin{Bmatrix} \mathbf{f} \\ \mathbf{0} \end{Bmatrix} \tag{35}$$

where $\mathbf{d}$ is the vector of nodal displacement variables and $\mathbf{p}$ is the vector of nodal pressure variables.

It is noted that the final set of governing equations exhibits the classical (u, p) form of coupled FE/FE vibro-acoustic problems and, in contrast with the uncoupled structural finite element model, the matrices of the plate coupled with the fluid are no longer symmetric. This is due to the fact that the force loading of the fluid on the structure is proportional to the pressure, resulting in a cross-coupling matrix $\mathbf{S}$ in the coupled stiffness matrix, while the force loading of the structure on the fluid is proportional to the acceleration, resulting in a cross-coupling matrix $\rho_{\mathrm{f}}\mathbf{S}^{\mathrm{T}}$ in the coupled mass matrix.

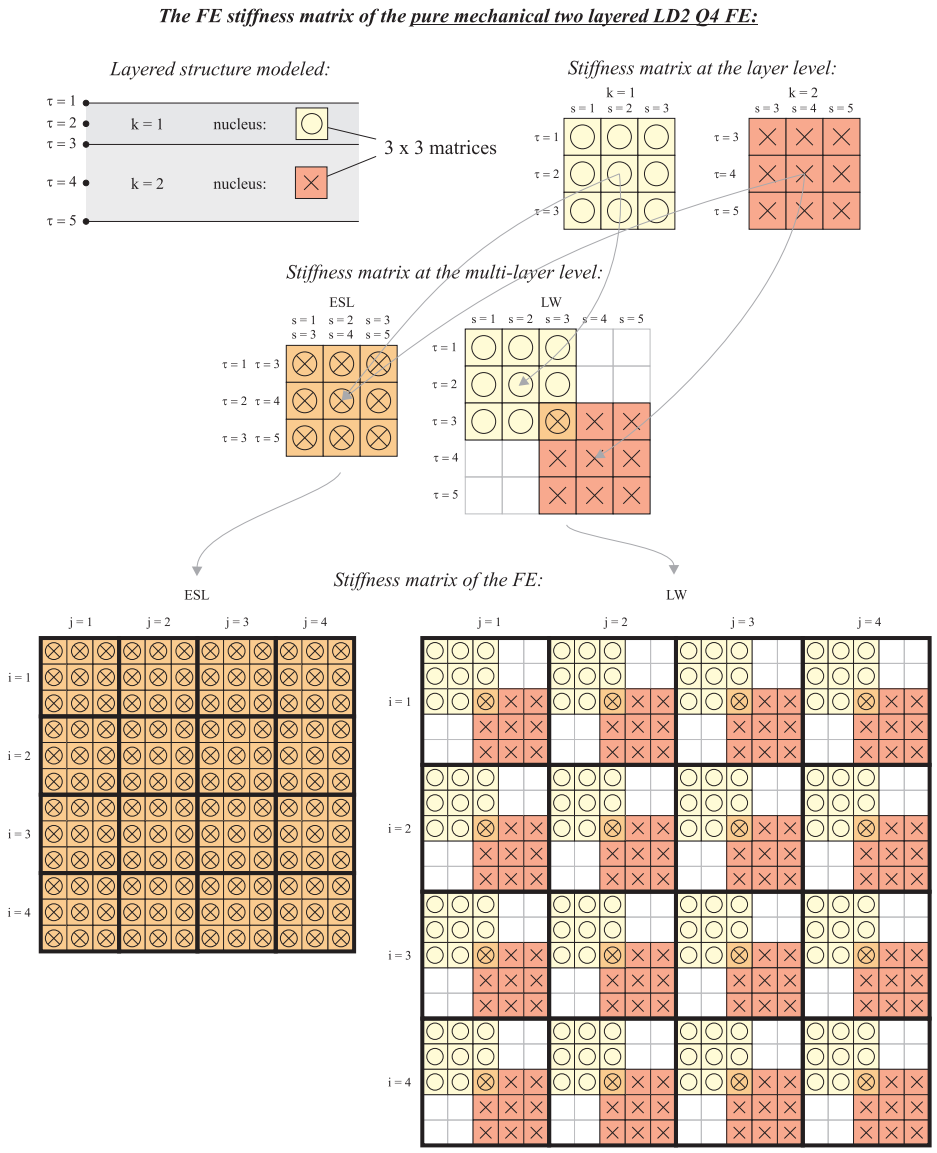

Figure 3: Example of the assembly procedure from the 3×3 stiffness nucleus to element level.

Note also that, for practical calculation, the coupled model in Eq. (35) is here computed with compatible acoustic and structural meshes, i.e., the nodes of the acoustic and the structural meshes at the fluid-structure coupling interface coincide. If not, the structural nodal displacement variables must be related to the acoustic nodal pressure variables along the fluid-structure interface through some geometrical transfer matrices.

4 Modal coupling solution

A direct time- or frequency-domain solution of the coupled equations (35) is computationally inefficient. This is due to the following reasons.

- The finite element matrices can be quite large, in particular when plates with many layers are modeled using layerwise theories of high order. Indeed, the 2-D higher-order kinematic models introduced in Section 3.2 can be substantially more accurate than classical plate models in approximating the true 3-D deformation field of the multilayered composite plate. However, refined models are obtained with 2-D elements which can have many more structural degrees of freedom per node than common plate elements relying on CPT or FSDT.

- The banded, sparsely populated and symmetric nature of the matrices in the uncoupled problem is lost due to the cross-coupling terms of the coupled finite element model. As a result, efficient solvers for sparse symmetric matrices must be replaced by non-symmetric solvers, which are more time expensive.

The computational effort can be highly reduced by using appropriate model order reduction techniques. The technique adopted in this work relies on a modal coupling solution [15]. According to this approach, the system is decomposed into two subsystems, i.e., the elastic multilayered plate and the acoustic fluid domain. The structural degrees of freedom are expanded in terms of a set of n_{s} *in vacuo* modes of the plate, i.e., the modes of the plate without the loading of the acoustic pressure, which are calculated by solving the structural symmetric eigenvalue problem

$$\left(\mathbf{K} - \omega^2 \mathbf{M}\right) \mathbf{d} = \mathbf{0} \tag{36}$$

Similarly, the acoustic degrees of freedom are expanded in terms of n_{a} rigid acoustic modes, i.e., the modes of the fluid domain with the fluid-structure interface assumed to be perfectly rigid, which are calculated by solving the acoustic symmetric eigenvalue problem

$$\left(\mathbf{H} - \omega^2 \mathbf{Q}\right) \mathbf{p} = \mathbf{0} \tag{37}$$

Accordingly, we can write

$$\left\{ \begin{array}{c} \mathbf{d} \\ \mathbf{p} \end{array} \right\} = \left[\begin{array}{cc} \mathbf{U}_{\mathrm{s}} & \mathbf{0} \\ \mathbf{0} & \mathbf{U}_{\mathrm{a}} \end{array} \right] \left\{ \begin{array}{c} \mathbf{q}_{\mathrm{s}} \\ \mathbf{q}_{\mathrm{a}} \end{array} \right\} \tag{38}$$

which is the relationship describing the transformation from the physical basis of nodal displacement and pressure coordinates to the modal basis of modal coordinates $\mathbf{q}_{\mathrm{s}}$ and $\mathbf{q}_{\mathrm{a}}$ through the structural and acoustic modal matrices $\mathbf{U}_{\mathrm{s}}$ and $\mathbf{U}_{\mathrm{a}}$. Substituting Eq. (38) into Eq. (35) and pre-multiplying the resulting equation with the transpose of the structural and acoustic modal matrices, the following model is obtained

$$\left[\begin{array}{cc} \mathbf{I}_{\mathrm{s}} & \mathbf{0} \\ \rho_{\mathrm{f}} \mathbf{U}_{\mathrm{a}}^{\mathrm{T}} \mathbf{S}^{\mathrm{T}} \mathbf{U}_{\mathrm{s}} & \mathbf{I}_{\mathrm{a}} \end{array} \right] \left\{ \begin{array}{c} \dfrac{\mathrm{d}^2 \mathbf{q}_{\mathrm{s}}}{\mathrm{d}t^2} \\ \dfrac{\mathrm{d}^2 \mathbf{q}_{\mathrm{a}}}{\mathrm{d}t^2} \end{array} \right\} + \left[\begin{array}{cc} \mathbf{\Lambda}_{\mathrm{s}} & -\mathbf{U}_{\mathrm{s}}^{\mathrm{T}} \mathbf{S} \mathbf{U}_{\mathrm{a}} \\ \mathbf{0} & \mathbf{\Lambda}_{\mathrm{s}} \end{array} \right] \left\{ \begin{array}{c} \mathbf{q}_{\mathrm{s}} \\ \mathbf{q}_{\mathrm{a}} \end{array} \right\} = \left\{ \begin{array}{c} \mathbf{U}_{\mathrm{s}}^{\mathrm{T}} \mathbf{f} \\ \mathbf{0} \end{array} \right\} \tag{39}$$

where $\mathbf{\Lambda}_{\mathrm{s}} = \mathrm{diag}\left(\ldots, \omega_{\mathrm{s}i}^2, \ldots\right)$ and $\mathbf{\Lambda}_{\mathrm{a}} = \mathrm{diag}\left(\ldots, \omega_{\mathrm{a}i}^2, \ldots\right)$ contain the uncoupled natural frequencies of the structural and acoustic domain $\omega_{\mathrm{s}i}$ and $\omega_{\mathrm{a}i}$, respectively, and the structural and acoustic modal vectors are assumed to be normalized with respect to their corresponding mass matrices, i.e., $\mathbf{U}_{\mathrm{s}}^{\mathrm{T}} \mathbf{M} \mathbf{U}_{\mathrm{s}} = \mathbf{I}_{\mathbf{s}}$ and $\mathbf{U}_{\mathrm{a}}^{\mathrm{T}} \mathbf{Q} \mathbf{U}_{\mathrm{a}} = \mathbf{I}_{\mathbf{a}}$.

The size of the modal model in Eq. (39) is substantially smaller than the model in Eq. (35) when a small truncated set of n_{s} structural and n_{a} acoustic modes yields a level of accuracy in the approximation of the dynamic response close to the one of the much larger original FE model. However, the efficiency of the modal coupling solution in reducing the size of the problem is typically rather poor since the uncoupled acoustic modes, which are calculated with rigid wall boundary condition at the plate interface, violate the related displacement continuity

condition. This yields an inaccurate representation of the near-field pressure effects in the vicinity of the fluid-plate coupling interface, which are usually associated with the displacement continuity. As shown below, the accuracy of the approximation can be improved by retaining a larger number of acoustic modes in the modal basis.

5 Numerical examples

In this section some illustrative numerical examples are presented and discussed to show the capabilities of the previous formulation.

5.1 Convergence of the structural model

First, the convergence properties of the uncoupled structural FE model are presented by considering a square laminated plate with clamped (C) edge conditions and having stacking sequence $[0°/90°/0°]$. The orthotropic material properties of the layers are the following: $E_1/E_2 = 40$, $E_3 = E_2$, $G_{12} = G_{13} = 0.6E_2$, $G_{23} = 0.5E_2$ and $\nu_{12} = \nu_{13} = \nu_{23} = 0.25$, where E_i is the Young's modulus along i-th direction, and G_{ij} and ν_{ij} are the corresponding shear modulus and Poisson's ratio, respectively. Each layer is assumed to be of equal thickness and mass density ρ. The first twelve non-dimensional frequency parameters $\lambda = \omega b\sqrt{\rho/E_2}$, where b is the side length of the plate, are listed in Table 1 and Table 2 corresponding to a thin ($h/b = 0.01$) and a moderately thick ($h/b = 0.1$) plate, respectively. Results are computed with models based on both ED and LD theories and are tabulated for increasing values of the order N of the theory and for increasing number (N_x, N_y) of 2-D four-node square elements along x and y directions. The total number of degrees of freedom n_{dof} corresponding to each model is also reported. Note that a selective reduced integration is employed to overcome the classical shear locking phenomenon [32].

It can be observed that, in both cases, the convergence is monotonic from above as the 2-D mesh is refined and the convergence rate is similar for ED and LD theories. Furthermore, well converged *in vacuo* frequency values are obtained when $N_x = N_y = 60$ for both thin and thick plates. It can be argued that the convergence rate is not significantly affected by the typology

and order of the assumed kinematic theory and by the thickness ratio h/b of the plate. This property has been also observed on plates having other boundary conditions and lamination layouts. It is also worth noting from Tables 1 and 2 that FE solutions yield different converged upper-bound values of the natural frequencies if different kinematic theories are selected. In particular, lower values are attained by increasing the order of the ED or LD theory and, for the same order N, ED theories yield higher frequency parameters than LD theories. Such differences are more marked as the thickness ratio of the plate increases and higher modes are considered. As shown in the next section, the typology of the kinematic theory, if layer independent or dependent, and the corresponding order N can strongly affect the accuracy of the solution.

5.2 Validation study

The FE models arising from the formulation described in Sections 3 and 4 are here validated against some reference studies available in the literature. Four cases are presented. The first three examples involve the validation of the *in vacuo* FE models by considering the free vibration analysis of rectangular thin and thick isotropic, laminated composite and sandwich plates with various boundary conditions. The last case study, instead, is related to the validation of the structural-acoustic response of an aluminum plate backed by an air-filled rigid-walled cubic cavity computed through the modal coupling solution.

The first case study involves a rectangular $a \times b$ isotropic plate with two opposite edges clamped (C) and the other two edges free (F). Two aspect ratios $a/b = 1$ and $a/b = 2$ are considered. For each aspect ratio, the *in vacuo* natural frequencies of plates with thickness ratio $h/b = 0.1$ and $h/b = 0.2$ are computed. Table 3 lists the first three frequency parameters $\lambda = \omega(b^2/\pi^2)\sqrt{\rho h/D}$, where D is the bending stiffness of the plate and ν is taken equal to 0.3, corresponding to symmetric-symmetric (SS), symmetric-antisymmetric (SA), antisymmetric-symmetric (AS), and antisymmetric-antisymmetric (AA) modes. Present values are computed with a mesh of 60×60 elements based on ED4 theory and are compared with Ritz solutions obtained by Liew et al. [36] through a fully 3-D vibration analysis. It can be observed that the present higher-order 2-D finite elements provide an excellent agreement with 3-D analysis in

Table 1: Convergence analysis of the first 12 modes of a CCCC square laminated plate with $h/b = 0.01$ and stacking sequence $[0°/90°/0°]$.

				mode number											
theory	N	$(N_x \times N_y)$	n_{dof}	1	2	3	4	5	6	7	8	9	10	11	12
ED	2	(10×10)	1089	0.4255	0.5221	0.7846	1.1755	1.2240	1.2900	1.3722	1.7301	2.1578	2.4156	2.4442	2.4634
	2	(20×20)	3969	0.4159	0.5031	0.7138	1.0638	1.1057	1.1523	1.2745	1.5174	1.5569	1.9151	2.1484	2.1807
	2	(30×30)	8649	0.4141	0.4997	0.7023	1.0305	1.0935	1.1397	1.2578	1.4785	1.4850	1.8436	2.0451	2.1042
	2	(40×40)	15129	0.4135	0.4985	0.6983	1.0192	1.0893	1.1354	1.2521	1.4527	1.4740	1.8200	1.9936	2.0891
	2	(50×50)	23409	0.4132	0.4980	0.6965	1.0141	1.0873	1.1334	1.2494	1.4410	1.4690	1.8093	1.9705	2.0822
	2	(60×60)	33489	0.4131	0.4977	0.6955	1.0113	1.0863	1.1323	1.2480	1.4347	1.4663	1.8036	1.9582	2.0784
	3	(60×60)	44652	0.4119	0.4964	0.6938	1.0083	1.0792	1.1252	1.2408	1.4291	1.4586	1.7941	1.9481	2.0563
	4	(60×60)	55815	0.4119	0.4964	0.6938	1.0083	1.0792	1.1252	1.2408	1.4291	1.4586	1.7941	1.9480	2.0563
LD	1	(10×10)	1452	0.4248	0.5214	0.7831	1.1705	1.2190	1.2843	1.3668	1.7215	2.1383	2.3970	2.4251	2.4422
	1	(20×20)	5292	0.4153	0.5025	0.7129	1.0613	1.1015	1.1482	1.2704	1.5124	1.5504	1.9069	2.1347	2.1669
	1	(30×30)	11532	0.4135	0.4992	0.7015	1.0283	1.0895	1.1358	1.2540	1.4731	1.4805	1.8366	2.0336	2.0912
	1	(40×40)	20172	0.4129	0.4980	0.6976	1.0172	1.0853	1.1315	1.2483	1.4477	1.4696	1.8134	1.9831	2.0764
	1	(50×50)	31212	0.4126	0.4975	0.6958	1.0122	1.0834	1.1296	1.2457	1.4362	1.4647	1.8029	1.9605	2.0695
	1	(60×60)	44652	0.4125	0.4972	0.6948	1.0094	1.0824	1.1285	1.2442	1.4300	1.4620	1.7972	1.9483	2.0658
	2	(60×60)	78141	0.4118	0.4963	0.6935	1.0075	1.0792	1.1251	1.2406	1.4272	1.4580	1.7926	1.9445	2.0562
	3	(60×60)	111630	0.4118	0.4963	0.6932	1.0067	1.0791	1.1250	1.2404	1.4254	1.4573	1.7911	1.9411	2.0560
	4	(60×60)	148840	0.4118	0.4963	0.6932	1.0067	1.0791	1.1250	1.2404	1.4254	1.4573	1.7911	1.9411	2.0560

Table 2: Convergence analysis of the first 12 modes of a CCCC square laminated plate with $h/b = 0.1$ and stacking sequence $[0°/90°/0°]$.

				mode number											
theory	N	$(N_x \times N_y)$	n_{dof}	1	2	3	4	5	6	7	8	9	10	11	12
ED	2	(10×10)	1089	2.2765	3.2248	4.3823	4.9301	5.0171	6.2124	6.9552	7.2637	7.4552	8.0989	8.2364	9.5974
	2	(20×20)	3969	2.2590	3.1410	4.3115	4.7117	4.8514	6.0000	6.7227	6.7371	7.0913	7.6820	7.9101	9.0256
	2	(30×30)	8649	2.2557	3.1260	4.2984	4.6584	4.8366	5.9618	6.5964	6.6968	7.0581	7.5846	7.8720	8.7838
	2	(40×40)	15129	2.2545	3.1208	4.2938	4.6400	4.8314	5.9485	6.5529	6.6826	7.0463	7.5509	7.8584	8.7008
	2	(50×50)	23409	2.2540	3.1184	4.2917	4.6315	4.8290	5.9423	6.5329	6.6761	7.0409	7.5353	7.8521	8.6626
	2	(60×60)	33489	2.2537	3.1171	4.2905	4.6269	4.8277	5.9390	6.5220	6.6726	7.0379	7.5269	7.8487	8.6420
	3	(60×60)	44652	2.1334	2.9349	4.0661	4.2872	4.5670	5.5596	5.9527	6.3362	6.6791	6.9463	7.4030	7.7963
	4	(60×60)	55815	2.1329	2.9335	4.0651	4.2830	4.5651	5.5550	5.9428	6.3344	6.6765	6.9360	7.3977	7.7765
	5	(60×60)	66978	2.1271	2.9049	4.0560	4.2166	4.5426	5.5025	5.8354	6.3159	6.6499	6.8452	7.3497	7.6324
	6	(60×60)	78141	2.1271	2.9048	4.0560	4.2163	4.5425	5.5023	5.8347	6.3158	6.6498	6.8447	7.3495	7.6310
	7	(60×60)	89304	2.1238	2.8902	4.0512	4.1842	4.5308	5.4766	5.7853	6.3076	6.6371	6.8023	7.3263	7.5677
LD	1	(10×10)	1452	2.1956	3.0360	4.2496	4.5834	4.7305	5.8140	6.6908	6.7699	7.0365	7.5301	7.7229	8.9588
	1	(20×20)	5292	2.1797	2.9686	4.1786	4.3370	4.6607	5.6482	6.0746	6.5451	6.8615	7.0792	7.5594	8.0670
	1	(30×30)	11532	2.1767	2.9565	4.1654	4.2940	4.6475	5.6181	5.9698	6.5038	6.8282	7.0012	7.5259	7.8594
	1	(40×40)	20172	2.1757	2.9523	4.1608	4.2791	4.6428	5.6075	5.9338	6.4894	6.8165	6.9743	7.5140	7.7885
	1	(50×50)	31212	2.1752	2.9503	4.1587	4.2723	4.6407	5.6027	5.9172	6.4827	6.8110	6.9619	7.5085	7.7561
	1	(60×60)	44652	2.1749	2.9493	4.1575	4.2686	4.6395	5.6000	5.9082	6.4791	6.8081	6.9551	7.5054	7.7385
	2	(60×60)	78141	2.1307	2.9088	4.0693	4.2221	4.5553	5.5153	5.8436	6.3440	6.6770	6.8594	7.3759	7.6442
	3	(60×60)	111630	2.1221	2.8822	4.0504	4.1672	4.5259	5.4640	5.7599	6.3077	6.6345	6.7815	7.3177	7.5367
	4	(60×60)	148840	2.1217	2.8818	4.0490	4.1667	4.5246	5.4628	5.7594	6.3047	6.6316	6.7803	7.3151	7.5359

all cases.

The second comparison study is referred to a square laminated $[0°/90°/0°]$ plate with $h/b = 0.1$ and three different Lévy-type boundary conditions with at least two opposite edges simply-supported. The three layers of equal thickness have the following dimensionless material properties: $E_1/E_2 = 40$, $E_3 = E_2$, $G_{12} = G_{13} = 0.6E_2$, $G_{23} = 0.5E_2$ and $\nu_{12} = \nu_{13} = \nu_{23} = 0.25$. The fundamental frequency parameter $\lambda = (\omega b^2/h)\sqrt{\rho/E_2}$ is shown in Table 4 for modes having $m = 1, 2, 3$ half waves in the y direction. Present results are reported when the plate is modeled using 40×40 structural elements based on ED7 and LD4 theories and are compared to those computed using a semi-analytical 3-D approach [37] and the exact Lévy method [38]. It is noted that FE models based on LD4 provide natural frequencies very close to reference 3-D and exact values even when $m = 3$. The fundamental frequency is slightly overestimated by ED7 models and it can be observed that the error increases at higher m values. This is a general behavior and is due to the fact that higher order modes of laminated plates are more and more characterized by a C^0 zig-zag form of the displacements in the thickness direction, which is not accurately captured by ESL theories.

In the last uncoupled structural example, a fully simply-supported square sandwich plate with soft-core is presented. The plate has a $[0^o/90^o/\text{core}/0^o/90^o]$ layup with material properties of the faces and the core listed in Table 5. The thickness of the core is assumed to be ten times the thickness of the face sheets. For the sake of comparison with results provided in [39], both thin ($h/b = 0.01$) and moderately thick ($h/b = 0.1$) plates are considered. *In vacuo* free vibration results are shown in Table 6 in terms of the non-dimensional frequency $\lambda = (\omega b^2/h)\sqrt{\rho/E_2}$ for some modes with (m, n) half waves along x and y direction, respectively. FE solutions obtained by the present formulation with a mesh of 60×60 elements are computed using a third-order ESL theory and four layerwise theories of increasing order. Table 6 clearly shows that models based on ED3 grossly overestimate the natural frequencies in comparison with models based on LD theories both for thin and moderately thick plates. This is due to the large difference in the stiffness between the skins and the core. Indeed, in this example the face-to-core-stiffness ratio (FCSR) E_1/E_c is approximately equal to 10^4. In the case of a flexible or soft-core (for example, a foam core) sandwich plate, difficulties are known in capturing the

Table 3: Frequency parameters of an isotropic plate with CFCF boundary conditions.

			mode											
a/b	h/b	Solution method	SS-1	SS-2	SS-3	SA-1	SA-2	SA-3	AS-1	AS-2	AS-3	AA-1	AA-2	AA-3
1	0.1	Present – ED4	2.1043	3.9229	9.7328	5.3864	7.3583	10.634	2.4481	5.9498	6.9693	5.8276	10.072	10.963
		3-D Ritz [36]	2.1050	3.9234	9.7276	5.3859	7.3581	10.636	2.4489	5.9500	6.9678	5.8272	10.070	10.961
	0.2	Present – ED4	1.8007	3.1922	5.8794	4.1108	5.3319	5.4665	2.0375	2.9770	5.4346	4.4128	5.4834	6.5934
		3-D Ritz [36]	1.7996	3.1909	5.8790	4.1062	5.3313	5.4625	2.0363	2.9770	5.4325	4.4084	5.4824	6.5929
2	0.1	Present – ED4	0.5486	2.6073	2.8295	1.4803	3.6565	4.5353	0.8670	2.6554	3.3588	1.9563	5.0729	5.2170
		3-D Ritz [36]	0.5492	2.6076	2.8300	1.4811	3.6575	4.5324	0.8677	2.6560	3.3596	1.9573	5.0707	5.2162
	0.2	Present – ED4	0.5222	2.3072	2.4187	1.3369	2.6553	3.0723	0.7885	1.3289	2.8102	1.7136	2.6088	4.0499
		3-D Ritz [36]	0.5224	2.3071	2.4174	1.3367	2.6556	3.0720	0.7884	1.3291	2.8090	1.7135	2.6083	4.0462

Table 4: Fundamental frequency for modes having m half waves along y direction of a $[0°/90°/0°]$ SSSS square laminated plate with $h/b = 0.1$.

		Boundary conditions		
m	Solution method	CSCS	CSSS	CSFS
1	Present – ED7	19.830	17.213	7.304
	Present – LD4	19.820	17.205	7.299
	3-D DQ [37]	19.809	17.195	7.256
	2-D Exact [38]	19.811	17.197	7.297
2	Present – ED7	25.152	23.362	17.068
	Present – LD4	25.109	23.319	17.015
	3-D DQ [37]	25.085	23.289	16.998
	2-D Exact [38]	25.086	23.292	16.977
3	Present – ED7	37.182	36.162	32.225
	Present – LD4	37.033	36.011	32.057
	3-D DQ [37]	36.908	35.877	31.929
	2-D Exact [38]	36.909	35.878	31.901

correct dynamic behavior with simple kinematic models [40, 41]. The numerical study shows that layerwise kinematics are required for sandwich plates with very soft core irrespective of the thickness-to-length ratio. It is also observed that a slight improvement in accuracy of natural frequencies is obtained by LD2 compared to LD1 theory, whereas no further improvement is detected by using a layerwise model of higher order.

Table 5: Material properties of the sandwich plate discussed in Section 5.2.

Component	Elastic modulus (GPa)	Poisson's ratio	Shear modulus (GPa)	Density (kg/m^3)
Face sheets	$E_1 = 131$	$\nu_{12} = 0.22$	$G_{12} = 6.895$	$\rho = 1627$
	$E_2 = 10.34$	$\nu_{13} = 0.22$	$G_{13} = 6.205$	
	$E_3 = 10.34$	$\nu_{23} = 0.49$	$G_{23} = 6.895$	
Core	$E_c = 6.89 \times 10^{-3}$	$\nu_c = 0$	$G_c = 3.45 \times 10^{-3}$	$\rho_c = 97$

As a final validation study of the present formulation, a coupled structural-acoustic case is now considered. The system consists of a cubic cavity of dimensions $1 \times 1 \times 1\,\mathrm{m}^3$, completely filled with air (speed of sound $c_\mathrm{f} = 343\,\mathrm{m/s}$, mass density $\rho_\mathrm{f} = 1.2\,\mathrm{Kg/m}^3$). Five walls of the cavity are assumed to be perfectly rigid. The top one is a simply-supported 1×1 m^2 flexible aluminium plate with thickness $h = 0.01$ m. The mechanical properties of the plate are the following: Young's modulus $E = 70\,\mathrm{GPa}$, mass density $\rho_s = 2700\,\mathrm{Kg/m}^3$ and Poisson's

Table 6: Nondimensional frequency parameters of a simply-supported square sandwich plate with material properties listed in Table 5.

			Present FE models					
h/b	m	n	ED3	LD1	LD2	LD3	LD4	Ref. [39]
0.01	1	1	15.5502	11.9484	11.9479	11.9479	11.9479	11.9401
	1	2	39.2996	23.4278	23.4259	23.4259	23.4259	23.4017
	1	3	73.6409	36.2093	36.2033	36.2033	36.2033	36.1434
	2	2	55.1923	30.9735	30.9694	30.9694	30.9694	30.9432
	2	3	84.4155	41.5039	41.4951	41.4951	41.4951	41.4475
	3	3	106.736	49.8233	49.8090	49.8090	49.8090	49.7622
0.1	1	1	4.9620	1.8543	1.8492	1.8492	1.8492	1.8480
	1	2	8.1952	3.2402	3.2233	3.2233	3.2233	3.2196
	1	3	11.997	5.2730	5.2363	5.2360	5.2360	5.2234
	2	2	10.520	4.3252	4.2946	4.2945	4.2945	4.2894
	2	3	13.759	6.1582	6.1075	6.1071	6.1071	6.0942
	3	3	16.467	7.7670	7.6964	7.6959	7.6959	7.6762

ratio $\nu = 0.35$. A transverse force of amplitude $1\,\mathrm{N}$ over the frequency range $[0, 300]$ Hz is applied on the plate at coordinates $(0.25\,\mathrm{m}, 0.35\,\mathrm{m})$. Assuming no damping in the structural and acoustic domain, the frequency response of the system under study is computed through the modal coupling solution described in Section 4 by solving the following set of equations

$$\left(\begin{bmatrix} \mathbf{\Lambda}_\mathrm{s} & -\mathbf{U}_\mathrm{s}^\mathrm{T}\mathbf{S}\mathbf{U}_\mathrm{a} \\ \mathbf{0} & \mathbf{\Lambda}_\mathrm{s} \end{bmatrix} - \omega^2 \begin{bmatrix} \mathbf{I}_\mathrm{s} & \mathbf{0} \\ \rho_\mathrm{f}\mathbf{U}_\mathrm{a}^\mathrm{T}\mathbf{S}^\mathrm{T}\mathbf{U}_\mathrm{s} & \mathbf{I}_\mathrm{a} \end{bmatrix} \right) \begin{Bmatrix} \mathbf{q}_\mathrm{s} \\ \mathbf{q}_\mathrm{a} \end{Bmatrix} = \begin{Bmatrix} \mathbf{U}_\mathrm{s}^\mathrm{T}\mathbf{f} \\ \mathbf{0} \end{Bmatrix} \tag{40}$$

In particular, the following quantities are evaluated:

- the acoustic pressure inside the cavity at coordinates $(0.75\,\mathrm{m}, 0.25\,\mathrm{m}, 0.75\,\mathrm{m})$, denoted as point A;
- the acoustic pressure inside the cavity at coordinates $(0.75\,\mathrm{m}, 0.25\,\mathrm{m}, 0.95\,\mathrm{m})$, denoted as point B;
- the specific kinetic energy of the plate defined as

$$E_\mathrm{kin} = \frac{1}{2}\frac{\omega^2}{\Omega_\mathrm{s}} \int_{\Omega_\mathrm{s}} \rho_\mathrm{s} |\boldsymbol{s}|^2 \,\mathrm{d}v = \frac{1}{2}\frac{\omega^2}{\Omega_\mathrm{s}} \mathbf{q}_\mathrm{s}^* \mathbf{q}_\mathrm{s} \tag{41}$$

where * denotes the complex conjugate operator;

- the acoustic mean-square pressure defined as

$$E_{\mathrm{p}} = \frac{1}{2}\frac{1}{\Omega_{\mathrm{f}}}\int_{\Omega_{\mathrm{f}}} |p|^2 \,\mathrm{d}v = \frac{1}{2}\frac{c_{\mathrm{f}}^2}{\Omega_{\mathrm{f}}}\mathbf{q}_{\mathrm{a}}^*\mathbf{q}_{\mathrm{a}} \tag{42}$$

Concerning the finite element discretization, structural and acoustic meshes compatible at the interface are used with 20 elements along each side. Since the plate is thin and isotropic, accurate solutions can be obtained with plate elements based on a low-order ESL theory. Results are shown in the following with ED2 models, which yield the same response of models of higher order in the frequency range under study. The convergence and accuracy of the modal coupling solution are studied by increasing the number of uncoupled structural n_{s} and acoustic n_{a} modes retained in the reduced modal basis and comparing the present response with the full direct solution available in [42].

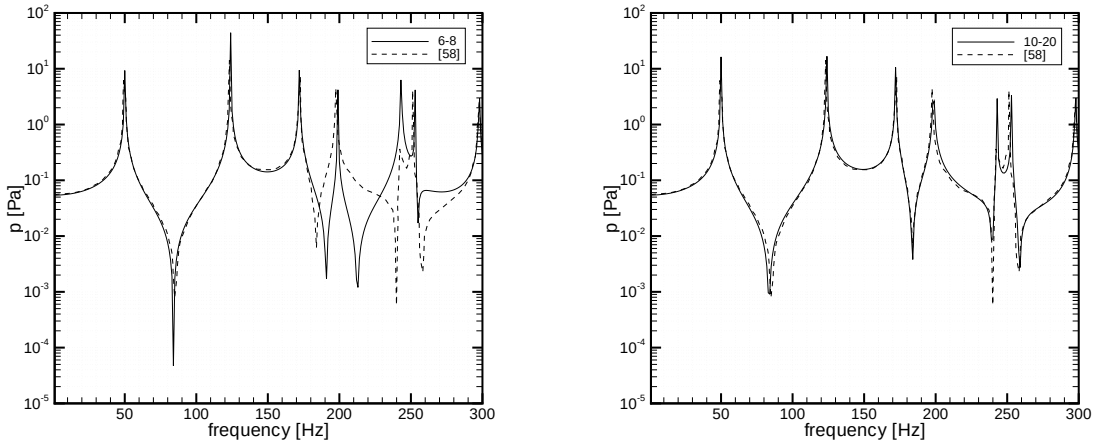

(a) $n_{\mathrm{s}} = 6, n_{\mathrm{a}} = 8$ (b) $n_{\mathrm{s}} = 10, n_{\mathrm{a}} = 20$

Figure 4: Pressure response at point A. Convergence of the modal coupling solution and comparison with the full order solution in [42].

Figure 4(a) shows the pressure response at point A with $n_{\mathrm{s}} = 6$ and $n_{\mathrm{a}} = 8$, corresponding to structural and acoustic modes falling within the frequency range of interest $[0, 300]$ Hz. Figure 4(b) shows the same response when $n_{\mathrm{s}} = 10$ structural modes and $n_{\mathrm{a}} = 20$ acoustic modes up to 450 Hz are included in the modal expansion. The dashed line represents the full-order reference solution used to validate the present model. It can be observed that the resonance peaks

of the pressure response are estimated with good accuracy even when only the modes below $300\,\mathrm{Hz}$ are considered, whereas the convergence of the anti-resonances appears to be slower and more modes should be retained in the reduced model to achieve an acceptable approximation. Note also that, as expected, low-frequency modes converge first than high-frequency modes. The converged result shows an excellent agreement with the reference solution and enables us to check the validity of the proposed fluid-structure coupling formulation.

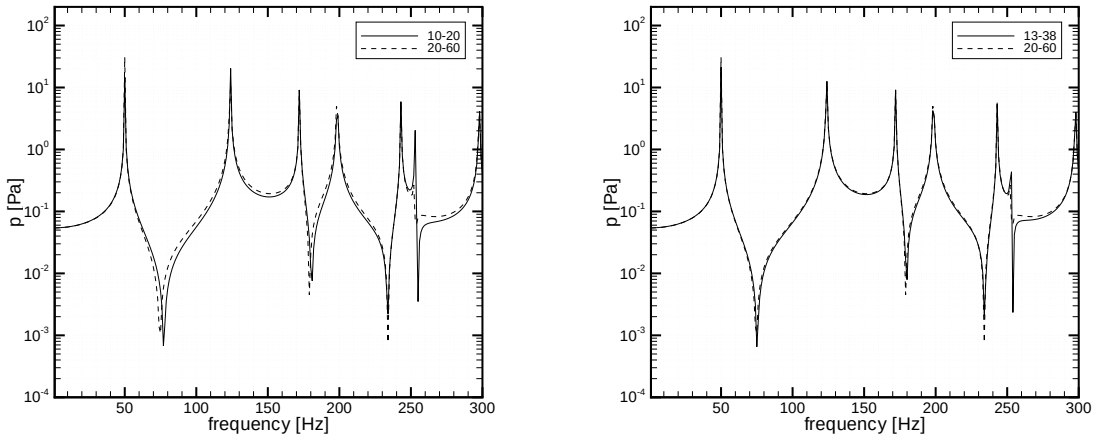

(a) $n_\mathrm{s} = 10, n_\mathrm{a} = 20$ (b) $n_\mathrm{s} = 13, n_\mathrm{a} = 38$

Figure 5: Pressure response at point B. Convergence of the modal coupling solution with respect to a modal solution with $n_\mathrm{s} = 20$ and $n_\mathrm{a} = 60$.

Figure 5 shows the convergence of the pressure response at point B, which is close to the plate-fluid interface. No reference solution is available for this response, so the convergence is evaluated with respect to a modal solution comprising $n_\mathrm{s} = 20$ and $n_\mathrm{a} = 60$ modes. It is noted that, as expected, the convergence now appears slightly slower than the previous case, since more acoustic modes are required to achieve an accurate local description in the vicinity of the structural-acoustic interface.

Finally, in Figure 6 the convergence of the structural and acoustic energy parameters introduced in Eq. (41) and (42) is shown. It is clear that the plate kinetic energy and the fluid potential energy converge faster than the previous pressure responses. This is expected since global quantities are typically estimated more accurately and efficiently than local quantities with the modal coupling technique.

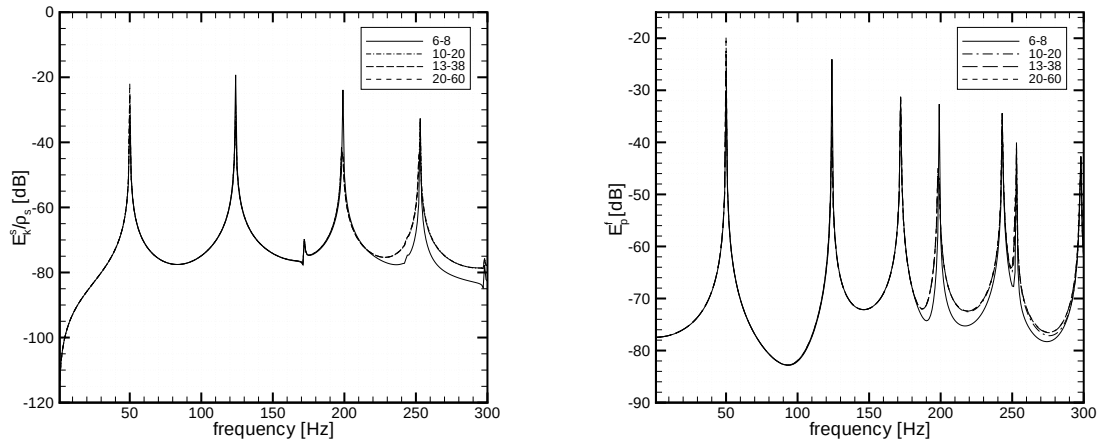

(a) plate kinetic energy

(b) mean-square pressure

Figure 6: Response in terms of energy parameters. Convergence of the modal coupling solution with respect to a modal solution with $n_{\mathrm{s}} = 20$ and $n_{\mathrm{a}} = 60$.

5.3 Frequency response of a sandwich plate coupled with an acoustic cavity

In this last section, a coupled structural-acoustic system consisting of a rectangular sandwich plate backed by a rigid cubic cavity is considered (see Figure 7). The example is aimed at showing the power and versatility of the present formulation in easily selecting the most appropriate structural model according to the accuracy requirements of the vibro-acoustic problem. In particular, a sandwich plate with a thick soft core is presented in order to highlight the advantages of higher-order kinematic models in improving the accuracy of the dynamic response.

Table 7: Properties of the sandwich plate discussed in Section 5.3.

Component	Parameter	Value
Plate	Length (a)	0.6 m
	Width (b)	0.4 m
	Boundary conditions	CCCC
	Layout	[face/core/face]
	h/a	0.01
Faces	Young's modulus (E_f)	73 GPa
	Poisson's ratio (ν_f)	0.34
	Density (ρ_f)	2800 kg/m^3
Core	Young's modulus (E_c)	variable
	Poisson's ratio (ν_c)	0.01
	Density (ρ_c)	30 kg/m^3
	Thickness (t_c)	$10\,t_f$

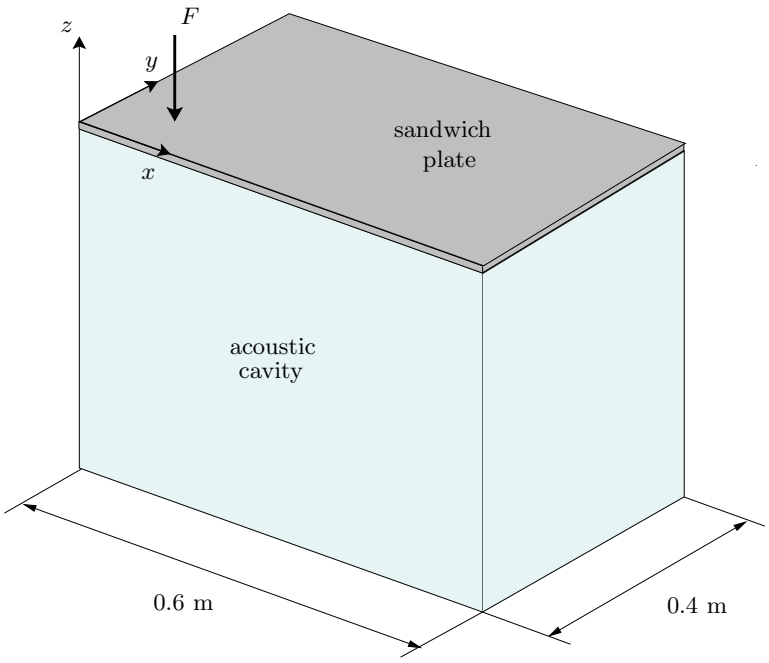

Figure 7: The plate-cavity system under study in Section 5.3.

The three-layered plate has the properties listed in Table 7. The faces are made of aluminum and the isotropic core has a variable Young's modulus $E_c = E_f/\mathrm{FCSR}$. Two cases are considered:

1. a sandwich plate with a relatively soft core having $\mathrm{FCSR} = 10^3$ (case 1);

2. a sandwich plate with a very soft core having $\mathrm{FCSR} = 10^5$ (case 2).

Even if this way of reducing mechanical properties is not physically sound, it appears to be reasonable within the framework and aim of this analysis.

As shown above for the *in vacuo* free vibration response, sandwich plates with a high stiffness ratio between the faces and the core (FCSR) require the use of layerwise kinematics to obtain reliable structural models, even when small thickness ratios are considered. Therefore, results are here shown with structural elements based only on LD theories. In particular, solutions are reported in the following for LD1 and LD3 models. It has been checked that models based on LD4 show no improvement compared to LD3 in the accuracy of the computations involved in the present analysis.

Each sandwich plate case is coupled with an air-filled cubic acoustic cavity having the other five faces assumed to be perfectly rigid. For case 1, the cavity has a depth of $0.5\,\mathrm{m}$,

whereas a cavity of depth $2.1\,\mathrm{m}$ is selected for case 2. Different cavities are considered since the plate with softer core has natural frequency values much lower than the case with a stiffer core. Consequently, with a larger cavity, some acoustic modes fall within the low-frequency spectrum of the system involving plate case 2 and the effect of the structural-acoustic coupling can be highlighted. Furthermore, case 1 is studied in the frequency range $[0, 800]$ Hz, including 6 structural modes and 11 acoustic modes. Instead, the frequency range of case 2 is limited to $300\,\mathrm{Hz}$ in order to have frequency response plots which are clearly readable without too many structural modes close each other.

The system is induced to vibrate by a unit transverse force acting on the top skin of the plate at coordinates $(0.08\,\mathrm{m}, 0.05\,\mathrm{m})$. The 2-D structural mesh involves 60×40 four-node elements for both cases. The cavity of case 1 is modeled with 10 hexahedral elements along its depth, whereas 20 elements are used for the cavity of case 2. The frequency-domain solution is obtained through the modal coupling technique presented in Section 4 by adding a small structural and acoustic modal damping as follows

$$\left(\begin{bmatrix} \mathbf{\Lambda}_\mathrm{s} & -\mathbf{U}_\mathrm{s}^\mathrm{T}\mathbf{S}\mathbf{U}_\mathrm{a} \\ \mathbf{0} & \mathbf{\Lambda}_\mathrm{s} \end{bmatrix} + j\omega \begin{bmatrix} \mathbf{C}_\mathrm{s} & \mathbf{0} \\ \mathbf{0} & \mathbf{C}_\mathrm{a} \end{bmatrix} - \omega^2 \begin{bmatrix} \mathbf{I}_\mathrm{s} & \mathbf{0} \\ \rho_\mathrm{f}\mathbf{U}_\mathrm{a}^\mathrm{T}\mathbf{S}^\mathrm{T}\mathbf{U}_\mathrm{s} & \mathbf{I}_\mathrm{a} \end{bmatrix} \right) \begin{Bmatrix} \mathbf{q}_\mathrm{s} \\ \mathbf{q}_\mathrm{a} \end{Bmatrix} = \begin{Bmatrix} \mathbf{U}_\mathrm{s}^\mathrm{T}\mathbf{f} \\ \mathbf{0} \end{Bmatrix} \tag{43}$$

where

$$\mathbf{C}_\mathrm{s} = \mathrm{diag}\,(\dots, 2\xi_{\mathrm{s}i}\omega_{\mathrm{s}i}, \dots) \qquad \mathbf{C}_\mathrm{a} = \mathrm{diag}\,(\dots, 2\xi_{\mathrm{a}i}\omega_{\mathrm{a}i}, \dots) \tag{44}$$

The modal damping factors are assumed to be $\xi_{\mathrm{s}i} = \xi_{\mathrm{a}i} = 0.01$.

First, the *in vacuo* frequency response of the two plate cases is presented in terms of kinetic energy. Figure 8(a) is referred to case 1, whereas the vibration response of case 2 is represented in Figure 8(b). The solid and dashed curves in each plot are obtained with LD1 and LD3 models, respectively. This preliminary *in vacuo* analysis is aimed at showing and explaining the differences between the uncoupled response and the coupled vibro-acoustic response presented in the following. It is observed that a first-order model is enough in estimating the correct kinetic energy for case 1 over the entire frequency range of interest. Case 2 shows that a rather accurate response is obtained by LD1 compared to LD3 model only in the very low-frequency

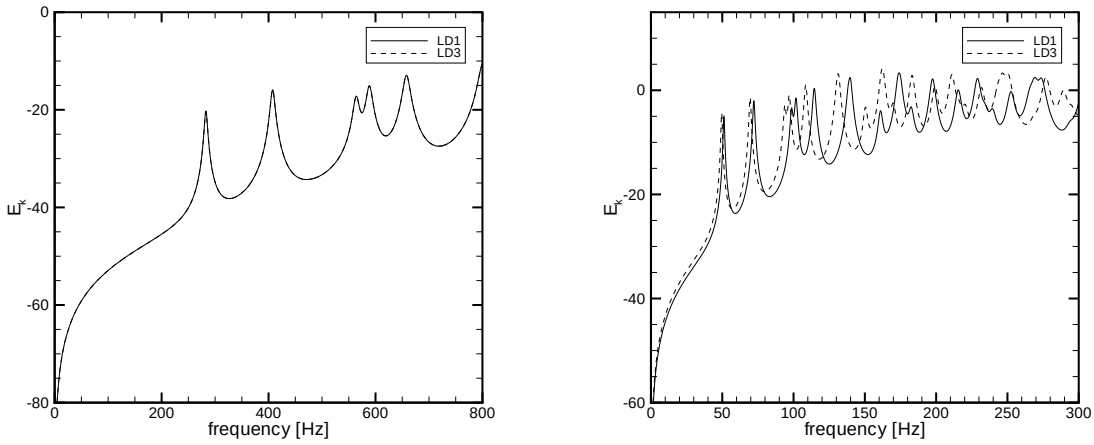

(a) Case 1 (b) Case 2

Figure 8: *In vacuo* frequency response functions in terms of kinetic energy of the sandwich plates.

portion of the spectrum, approximately below 100 Hz. Significant discrepancies are clearly visible at higher frequencies with an increasing shift of the resonance peaks as the frequency increases. A model based on LD3 is required for this case if good accuracy of the response is needed up to 300 Hz. However, it is also noted that the solid and dashed lines in Figure 8(b) are qualitatively similar, i.e., there are no missing modal contributions and the only difference is a shift of the modal peaks towards lower frequencies introduced by the LD3 model, which is capable of contrasting the stiffening effect of the linear LD1 model by capturing the nonlinear deformation field of the very soft core of the plate. This means that the modal participation factors of the *in vacuo* structural response are substantially unaffected by the refinement of the kinematic model.

The response of the system when the plate is coupled with the acoustic fluid in the cavity is shown in Figures 9 and 10.

Let us focus first on the kinetic energies of plate case 1 and 2, which are plotted in Fig. 9(a) and Fig. 10(a), respectively, using 2-D structural elements based on LD1 and LD3. First, it can be observed that, as expected, the coupled response exhibits resonance peaks corresponding to both plate-controlled modes and cavity-controlled modes. Plate-controlled modes are coupled modes similar to *in vacuo* plate modes with a small perturbation induced by the effect of the cavity pressure. Indeed, their natural frequencies are slightly lower than those of *in vacuo*

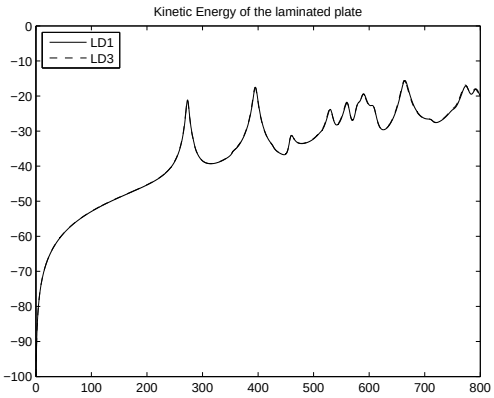

(a) Kinetic energy of the plate

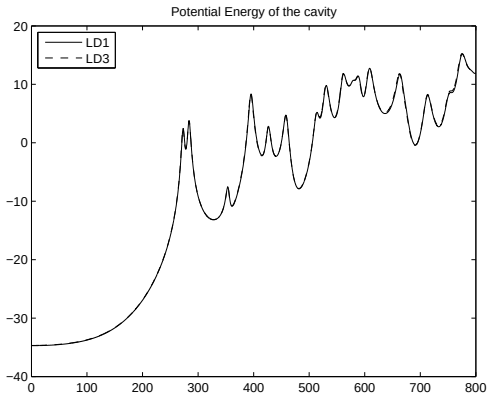

(b) Mean square pressure inside the cavity

Figure 9: Frequency response functions of the sandwich plate of case 1.

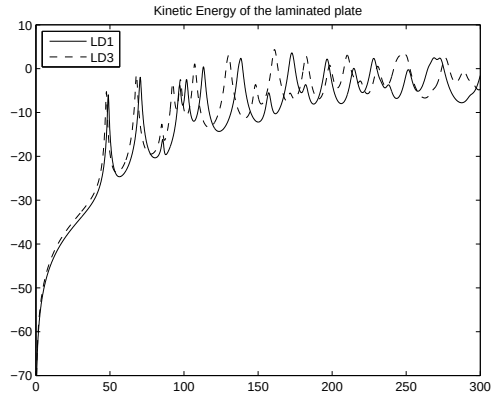

(a) Kinetic energy of the plate

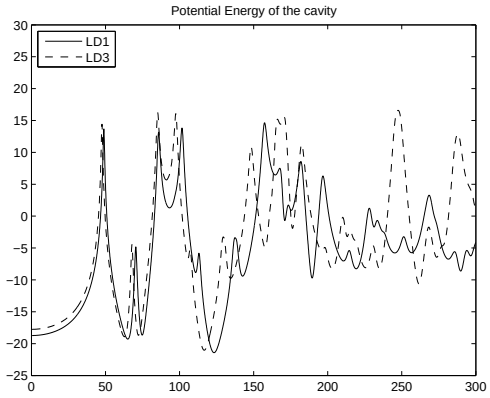

(b) Mean square pressure inside the cavity

Figure 10: Frequency response functions of the sandwich plate of case 2.

modes due to the added-mass effect of the fluid. On the contrary, cavity-controlled modes are coupled modes where the displacement of the plate is significantly distorted to match the pressure distribution of the enclosure. They appear as new resonance peaks in Figures 9(a)-10(a) compared to Figures 8(a)-8(b). It is also noted that no difference between LD1 and LD3 models is observed in the kinetic energy of the sandwich plate with stiffer core, whereas the kinetic energy computed with the model based on LD1 is substantially inaccurate for case 2 over a large portion of the frequency range under study.

When a measure of the pressure field inside the cavity is of interest, we can see from Figures 9(b) and 10(b) that the inaccuracy of LD1 model can introduce large errors in the estimation of the acoustic response. Indeed, the solid and dashed curves in Fig. 10(b) show unacceptable discrepancies above 150 Hz, in particular around 170, 250 and 290 Hz. This can be explained with the aid of Table 8, which lists the natural frequencies corresponding to coupled modes of case 2 up to 300 Hz computed with LD1 and LD3 models. The type of each coupled mode, if cavity-controlled or plate-controlled, is also reported. It is observed that the frequency regions where the difference between LD1 and LD3 curves is large correspond to cavity-controlled modes of the coupled system. The estimation of the natural frequency of such modes, which are dominated by the acoustic cavity, is only slightly affected by the model refinement of the elastic structure. On the contrary, since the pressure field must be compatible with the plate displacement at the fluid-structure interface, a wrong evaluation of the structural modal contributions surrounding the cavity-controlled mode involves the lost of spatial matching between the structural and the acoustic deformation patterns. As a result, the acoustic response is badly estimated. Furthermore, the higher is the modal density around the cavity-controlled modes, the higher is the error introduced by an inaccurate structural model.

6 Conclusions

In this work, the unified formulation introduced by Carrera has been extended to the numerical modeling of coupled structural-acoustic systems. In particular, a powerful and versatile finite-element tool for the accurate prediction of the low-frequency vibro-acoustic response of thin to

Table 8: Natural frequencies [Hz] of the coupled system for case 2. Letter C indicates cavity-controlled modes and letter P indicates plate-controlled modes.

	LD1		LD3	
mode number	frequency	mode type	frequency	mode type
1	0.00	C	0.00	C
2	48.87	P	47.61	P
3	70.46	P	67.88	P
4	85.80	C	85.16	C
5	97.06	P	92.38	P
6	101.72	P	97.57	P
7	113.14	P	107.23	P
8	137.03	P	129.11	P
9	138.50	P	130.32	P
10	157.24	P	14830	P
11	168.61	C	160.80	P
12	172.41	P	161.47	P
13	173.29	P	165.35	P
14	182.15	P	171.37	C
15	196.60	P	182.40	P
16	214.64	P	198.36	P
17	228.08	P	210.20	P
18	232.94	P	214.65	P
19	238.25	P	219.18	P
20	249.14	C	230.79	P
21	251.41	P	242.96	P
22	265.20	P	245.55	P
23	268.63	P	249.20	C
24	273.07	P	249.86	P
25	286.48	C	268.01	P
26	293.35	P	276.43	P
27	298.53	C	286.12	C
28	-	-	288.86	P
29	-	-	294.60	P
30	-	-	298.21	C

thick multilayered composite plates coupled with an acoustic fluid is developed. The main advantage of the proposed model relies in its invariant property with respect to the assumed plate theory, such that variable kinematic plate and fluid-structure interface elements can be easily obtained within a single mathematical framework. A large number of elements, based both on higher-order equivalent single-layer and layerwise theories, have been derived and implemented. The drawbacks related to the lack of symmetry of the adopted (u, p) formulation have been partially overcome by a modal coupling solution technique. Some examples describing the properties and capabilities of the proposed models have been discussed through the comparison with reference cases available in the literature. It has been also shown that refined plate elements are needed in some cases in order to correctly estimate the fluid-structure coupling and compute a reliable response of the vibro-acoustic system.

Acknowledgments

The authors wish to thank Prof. E. Carrera and people of his research staff (the MUL2 group) at Politecnico di Torino for their support at the early stages of this work.

References

[1] H.J.P. Morand, R. Ohayon, *Fluid-structure interaction*, John Wiley & Sons, 1995.

[2] R. Ohayon, C. Soize, *Sructural acoustics and vibration. Mechanical models, variational formulations and discretization*, Academic Press, 1998.

[3] R.J. Bernhard, M. Moeller, S. Young, Automobile, bus, and truck interior noise and vibration prediction and control, in: M.J. Crocker (Ed.), *Handbook of Noise and Vibration Control*, Wiley, New York, 2007.

[4] J.F. Wilby, Aircraft cabin noise and vibration prediction and passive control, in: M.J. Crocker (Ed.), *Handbook of Noise and Vibration Control*, Wiley, New York, 2007.

[5] J. Pan, D.A. Bies, The effect of fluid-structural coupling on sound waves in an enclosure – theoretical part, *Journal of the Acoustical Society of America*, 87 (1990), 691-707.

[6] C.R. Fuller, S.D. Snyder, C.H. Hansen, R.J. Silcox, Active control of interior noise in model aircraft fuselages using piezoceramic actuators, *AIAA Journal*, 30 (1992), 2613-2617.

[7] P. Gardonio, Review of active techniques for aerospace vibro-acoustic control, *Journal of Aircraft*, 39 (2002), 206-214.

[8] L. Dozio, G.L. Ghiringhelli, Experiments on active vibration and noise reduction of a panel using predictive techniques, *Structural Control and Health Monitoring*, 15 (2008), 1-19.

[9] N. Atalla, R.J. Bernhard, Review of numerical solutions for low-frequency structural-acoustic problems, *Applied Acoustics*, 43 (1994), 271-294.

[10] K.J. Bathe, *Finite Element Procedures*, Prentice Hall, 6th edition, 1996.

[11] F. Fahy, P. Gardonio, *Sound and structural vibration. Radiation, transmission and response*, Elsevier, 2n edition, 2007.

[12] J.-F. Deu, W. Larbi, R. Ohayon, Piezoelectric structural acoustic problems: symmetric variational formulations and finite element results, *Computer Methods in Applied Mechanical Engineering*, 197 (2008), 1715-1724.

[13] C.A. Felippa, R. Ohayon, Mixed variational formulation of finite element analysis of acoustoelastic/slosh fluid-structure interaction, *Journal of Fluids and Structures*, 4 (1990), 35-57.

[14] Z.-D. Ma, I. Hagiwara, Development of a new mode-superposition technique for modal frequency response analysis of coupled acoustic-structural systems, *Finite Elements in Analysis and Design*, 14 (1993), 209-223.

[15] G. Sandberg, A new strategy for solving fluid-structure problems, *Internation Journal for Numerical Methods in Engineering*, 38 (1995), 357-370.

[16] M. Tournour, N. Atalla, Pseudostatic corrections for the forced vibroacoustic response of a structure-cavity system, *Journal of the Acoustical Society of America*, 107 (2000), 2379-2386.

[17] E.H. Dowell, H.M. Voss, The effect of a cavity on panel vibration, *AIAA Journal*, 1 (1963), 476-477.

[18] L.P. Franzoni, D.B. Bliss, A discussion of modal uncoupling and an approximate closed-form solution for weakly-coupled systems with application to acoustics, *Journal of the Acoustical Society of America*, 103 (1998), 1923-1932.

[19] K.S. Sum, J. Pan, On acoustic and structural modal cross-couplings in plate-cavity systems, *Journal of the Acoustical Society of America*, 107 (2000), 2021-2038.

[20] Y.Y. Li, L. Cheng, Vibro-acoustic analysis of rectangular-like cavity with a tilted wall, *Applied Acoustics*, 68 (2007), 739-751.

[21] F. Casadei, L. Dozio, M. Ruzzene, K. A. Cunefare, Periodic shunted arrays for the control of noise reduction in an enclosure, *Journal of Sound and Vibration*, 329 (2010), 3632-3646.

[22] W. Larbi, J.-F. Deu, R. Ohayon, Finite element formulation of smart piezoelectric composite plates coupled with acoustic fluid, *Composite Structures*, 94 (2012), 501-509.

[23] E. Carrera, Theories and finite elements for multilayered, anisotropic, composite plates and shells, *Archives of Computational Methods in Engineering*, 9 (2002), 87-140.

[24] A.K. Noor, W.S. Burton, Assessment of shear deformation theories for multilayered composite plates, *Applied Mechanics Review*, 41 (1989), 1-18.

[25] J.N. Reddy, D.H. Robbins, Theories and computational models for composite laminates, *Applied Mechanics Review*, 47 (1994) 147-165.

[26] J.N. Reddy, R.A. Arciniega, Shear deformation plate and shell theories: from Stavsky to present, *Mechanics of Advanced Materials and Structures*, 11 (2004), 535-582.

[27] C. Wanji, W. Zhen, A selective review on recent development of displacement-based laminated plate theories, *Recent Patents on Mechanical Engineering*, 1 (2008), 29-44.

[28] Y.X. Zhang, C.H. Yang, Recent developments in finite element analysis for laminated composite plates, *Composite Structures*, 88 (2009), 147-157.

[29] E. Carrera, A class of two dimensional theories for multilayered plates analysis, *Atti Accademia delle Scienze di Torino. Memorie Scienze Fisiche*, 1920 (1995), 49-87.

[30] E. Carrera, An assessment of mixed and classical theories on global and local response of multilayered orthotropic plates, *Composite Structures*, 50 (2000), 183-198.

[31] E. Carrera, L. Demasi, Classical and advanced multilayered plate elements based upon PVD and RMVT. Part 1: Derivation of finite element matrices, *International Journal for Numerical Methods in Engineering*, 55 (2002), 191-231.

[32] E. Carrera, L. Demasi, Classical and advanced multilayered plate elements based upon PVD and RMVT. Part 2: Numerical implementations, *International Journal for Numerical Methods in Engineering*, 55 (2002), 253-296.

[33] E. Carrera, L. Demasi, M. Manganello, Assessment of Plate Elements on Bending and Vibrations of Composite Structures, *Mechanics of Advanced Materials and Structures*, 9 (2002), 333-357.

[34] A. Robaldo, E. Carrera, A. Benjeddou, A unified formulation for finite element analysis of piezoelectric adaptive plates, *Composite Structures*, 84 (2006), 1494-1505.

[35] J.N. Reddy, *Mechanics of laminated composite plates and shells*, CRC Press, 2004.

[36] K.M. Liew, K.C. Hung, M.K. Lim, A continuum three-dimensional vibration analysis of thick rectangular plates, *International Journal of Solids and Structures*, 30 (1993), 3357-3379.

[37] W.Q. Chen, C.F. Lue, 3D free vibration analysis of cross-ply laminated plates with one pair of opposite edges simply supported, *Composite Structures*, 69 (2005), 77-87.

[38] L. Dozio, Exact vibration solutions for cross-ply laminated plates with two opposite edges simply supported using refined theories of variable order, *Journal of Sound and Vibration*, 333 (2014), 2347-2359.

[39] M. K. Rao, Y. M. Desai, Analytical solutions for vibrations of laminated and sandwich plates using mixed theory, *Composite Structures*, 63 (2004), 361-373.

[40] Y. Frostig, O.T. Thomsen, Higher-order free vibration of sandwich panels with a flexible core, *International Journal of Solids and Structures*, 41 (2004), 1697-1724.

[41] E. Carrera, S. Brischetto, A survey with numerical assessment of classical and refined theories for the analysis of sandwich plates, *Applied Mechanics Review*, 62 (2009), 010803 1-17.

[42] R.S. Puri, *Krylov subspace based direct projection techniques for low frequency, fully coupled, structural acoustic analysis and optimization*, PhD thesis, Oxford Brookes University, 2008.